공학석사 학위논문

Seismic Earth Pressure Acting on Basement Walls of Buildings Using 1-g Shaking Table Model Test

1-g 진동대 모형실험을 이용한 건축물 지하벽체에 작용하는 동적토압

2023년 8월

서울대학교 대학원

건설환경공학부

황 태 훈

Seismic Earth Pressure Acting on Basement Walls of Buildings Using 1-g Shaking Table Model Test

지도 교수 김 성 렬

이 논문을 공학석사 학위논문으로 제출함

2023년 8월

서울대학교 대학원

건설환경공학부

황 태 훈

황태훈 석사 학위논문을 인준함

2023년 8월

위 원 장 정 충 기 (인)

부위원장 김 성 렬 (인)

위 원 박 준 범 (인)

Abstract

Analysis of Seismic Earth Pressure Acting on Basement Walls of Buildings Using 1-g Shaking Table Model Test

Hwang, Tae Hun
Department of Civil and Environmental Engineering
The Graduate School
Seoul National University

During earthquakes, seismic earth pressure acting on basement walls of buildings can have a significant impact on the stability of the structure. Seismic earth pressure is greatly influenced by the dynamic interaction between the ground and the structure. Numerous studies have been conducted to determine the seismic earth pressure acting on basement walls. Among them, the equivalent static analysis-based method has been predominantly used and adopted as the approach for determining seismic earth pressure in seismic design codes. Buildings with basements, constructed in urban areas, typically consist of superstructures composed of multiple stories. These buildings experience complex effects on seismic earth pressure acting on basement walls due to the interaction between the behaviors of the superstructure during earthquakes and the soil-structure interaction. However, the current equivalent

static analysis-based method completely disregards the influence of soil-structure interaction, even though the significance of this interaction is acknowledged in design codes. Therefore, there is a need for research that incorporates the influence of soil-structure interaction on seismic earth pressure acting on underground structures.

In this study, 1-g shaking table model experiments were conducted to analyze the influence of the number of the superstructure stories and the characteristics of the input waves on dynamic earth pressure. The model structures were carefully designed to satisfy the scaling laws for the prototype's natural frequency, height, and mass. Three model configurations were used based on the height of the superstructure: basement only, low-rise building with basements and high-rise building with basements. The model ground consisted of a compacted single layer of dense sandy soil with a relative density of approximately 80%, prepared using compaction technique with the shaking table.. The input waves were composed of 16 sinusoidal waves with varying frequencies and peak accelerations and were applied from the base of the soil box. The dynamic earth pressure was measured using loadcells installed on the outer walls of basement structure, while accelerometers and LVDTs were employed to measure the seismic response of the model ground and structure.

According to the experimental results, The horizontal responses of the structure increased with the number of stories in the superstructure. Furthermore, in case of basement only, the distribution of dynamic earth pressure exhibited a triangular shape that increased with depth within the ground. However, as the height of the superstructure increased, the dynamic earth pressure distribution gradually transformed into an inverted triangular shape, with larger values near the ground surface. Additionally, the proposed seismic earth coefficient, which takes into account the height of the superstructure, indicated that the dynamic earth pressure increases as the height of the superstructure increases. These values were significantly larger

compared to the predictions obtained using the existing methods that did not consider the influence of the superstructure. Finally, a seismic earth pressure coefficient based on the maximum ground surface acceleration and the number of superstructure levels was proposed.

Keywords: Basement walls, Seismic Earth Pressure, 1-g Shaking Table, Soil-Structure Interaction (SSI), Physical Modeling

Student Number: 2021-20334

Contents

List of Tables

List of Figures

Chapter 1 Introduction

1.1 Background

Until the early 2010s, Korea was perceived as a safe country in terms of earthquakes. However, the magnitude 5.8 Gyeongju earthquake on September 12, 2016, and the magnitude 5.4 Pohang earthquake on November 15, 2017, raised awareness among the public about the potential seismic risks and drew the attention of engineers. Table 1.1 presents statistical data on the number of domestic earthquakes by year, provided by the Korea Meteorological Administration. Prior to 2015, fewer than 60 earthquakes occurred on average per year. However, after the Gyeongju and Pohang earthquakes, the annual average increased to about 128 earthquakes from 2016 to 2022. Consequently, there is an emphasized need for specific seismic countermeasures for buildings.

Table 1.1 Number of Earthquakes in South Korea by year
(Provided by the Korea Meteorological Administration)

Year	$2.0 \le M < 3.0$	$3.0 \le M < 4.0$	$4.0 \le M < 5.0$	$5.0 \le M$	Total
1979-1989	75	96	11	3	185
1990-1999	162	77	14	0	253
2000-2009	349	75	8	2	434
2010-2015	277	54	4	1	336
2016-2022	803	78	8	4	893

On the other hand, with the advancement of science and technology leading to industrialization, there has been a global phenomenon of increased

population density in urban areas. Consequently, the number of high-rise buildings, including basement floors, has increased in order to secure residential space. According to statistical data from the Ministry of Land, Infrastructure and Transport (2019), which focused on high-rise buildings of 15 floors or more in South Korea, the number of buildings including basement floors accounted for approximately 58% of the total, indicating a significant presence of buildings with basement floors. While basement floors are generally considered safe from earthquakes due to their greater stiffness compared to the adjacent ground, numerous cases of damage to buildings with basements, have been reported both domestically and internationally, as shown in Figure 1.1. This highlights the need to ensure seismic stability for basement floors in practice.

Figure 1.1 Cases of substructure failure: (a) shear failure of columns in the substructure induced by Pohang earthquake in 2017 and (b) substructure failure by Hualien earthquake in 2018

The dynamic characteristics of a building can be influenced not only by its own dynamic properties but also by the surrounding ground. When seismic waves propagate through the ground where a structure is situated, the structure responds with various dynamic behaviors depending on its structural system and configuration. Consequently, the waves can influence the ground

response, which further affects the dynamic response of the structure. This interaction between the structure and the surrounding soil, leading to changes in the vibration characteristics of the structure, is known as Soil-Structure Interaction (SSI) (Figure 1.2)(NIST, 2012).

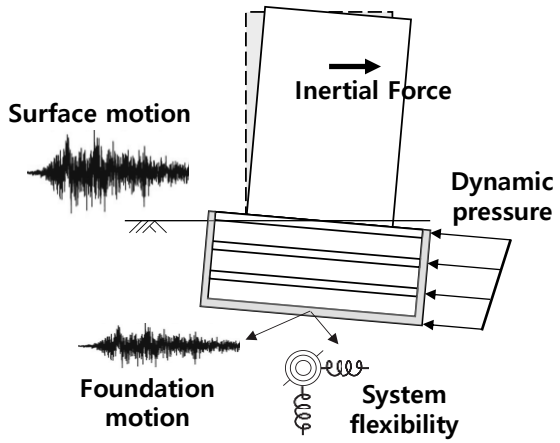

Figure 1.2 Effects of Soil-Structure-Interaction (SSI)

In this way, the ground-structure interaction plays a crucial role in the response of the entire system to seismic loads. However, despite the fact that basement structures are typically characterized by wide foundation widths and deep embedment depths, which significantly affect the dynamic interaction, there is a significant lack of consideration for this interaction in the estimation of dynamic earth pressures.

In the MOLIT(2019), it is suggested to apply the equivalent static method for estimating seismic earth pressures when the depth of soil from the ground surface to the bedrock is within 15m and the depth from the ground surface to the bottom of the basement structure's foundation is less than 2/3 of the soil depth. FEMA (2009) classifies basement structures into yielding walls and non-yielding walls based on their displacement behavior, and proposes the

use of the Mononobe-Okabe method for yielding walls. In this case, the distribution of dynamic earth pressures is assumed to follow an inverted triangular shape based on the research by Seed and Whitman (1970). For non-yielding walls, the method by Wood (1973) is suggested. ASCE (2016) indicates the need for further research on dynamic earth pressures in substructures but does not provide specific methods for their application. PEER (2017) mentions that considering the dynamic interaction among the ground, substructure, and superstructure can have both positive and negative effects on seismic safety, depending on various conditions such as the ground, foundation, and seismic waves. While there is no specific calculation method for seismic lateral earth pressures, classical methods (related to ground acceleration, Mononobe-Okabe method, and its variants) are discouraged due to their tendency to over-predict earth pressures.

To summarize, while some design codes utilize the M-O method-based equivalent static approach, concerns have been raised about the excessive estimation of dynamic earth pressures using the M-O method. However, it should be noted that the M-O method was originally developed for retaining walls and may not be suitable for applying to basements of large structures with significant superstructure mass. Furthermore, although considering soil-structure interaction (SSI) is important, the dynamic interaction between the ground, substructure, and superstructure can have both positive and negative effects on seismic safety, depending on various factors such as soil conditions, foundation design, and seismic waves. Due to these challenges, current seismic design codes lack specific design techniques in this regard. Therefore, there is a need for research on dynamic earth pressures acting on basement walls of buildings to develop seismic designs that consider the dynamic interaction among the ground, basement structure, and superstructure.

1.2 Objectives and Scope

Based on the above discussion, this study aims to analyze the effect of the superstructure on the dynamic earth pressure acting on the basement walls through a series of 1-g shaking table model experiments. In summary, the main objectives of the present study are as follows:

(1) Analyzing the dynamic responses of buildings based on the number of superstructure stories.
(2) Analyzing the distribution and magnitude variations of dynamic pressures based on the number of floors in the superstructure.
(3) Proposing a seismic earth pressure coefficient based on the maximum ground acceleration for the seismic design of basement structures, considering the number of floors in the superstructure.

The model used in this experiment is a building with basements based on SH (2019) design. The ground was modeled as a single layer of dry dense sand under horizontal conditions. The structure and ground modeled in the 1-g shaking table test are limited to the following conditions

- Because of small-scale restrictions, it is usually impossible to simultaneously comply with all the scaling factors. Therefore, the model was scaled by applying similarity laws only to the natural period, mass, and length, which are relevant physical properties of this

experiment.

- In order to focus on the influence of inertia forces according to the number of floors and mass of the upper structure, the model only simulated the columns and slabs of the prototype structure, while disregarding other components such as beams, finishes, and foundations.
- The model ground was constructed using silica sand corresponding to SP classification according to the Unified Soil Classification System. Since there was no specific prototype ground condition for the prototype, arbitrary ground conditions were applied in the experiment.
- To assess the effects of frequency and amplitude of the input wave, a sine waves were applied in the experiment.

1.3 Dissertation Organization

This dissertation comprises five chapters which are briefly introduced as follows:

In Chapter 1, the background, objectives and scope, and structure of dissertation are presented.

In Chapter 2, literature review on the dynamic earth pressures acting on basement walls of buildings is presented. It starts with an overview of analytical methods and their validation through experimental methods. The chapter also discusses recent studies that consider soil-structure interaction (SSI) and identifies research gaps in this field.

In Chapter 3, a series of processes involved in physical modeling is presented. It includes preliminary test to verify the boundary effect of a rigid box and efforts to simulate the characteristics of the prototype in the physical model. This chapter also discusses the purpose of instruments and provides the properties of the soil. Furthermore, it outlines the sequence of constructing the experimental section and presents the test program.

In Chapter 4, The evaluation of seismic earth pressures on basement walls of buildings is discussed. This chapter specifically examines the analysis of dynamic responses of buildings based on the number of superstructure stories. the influence of the superstructure's inertia on the seismic earth pressure distribution and magnitude is also examined. Additionally, a seismic earth pressure coefficient is proposed, taking into account the variable of the superstructure's number of stories.

Finally, in Chapter 5, the main conclusion of the dissertation and recommendations for further research are presented.

Chapter 2 Literature Review

2.1 Dynamic Earth Pressures on Basement Walls of Buildings

As discussed previously, both domestic and international design codes utilize the pseudo-static approaches which derived from Mononobe-Okabe (M-O) method. In the field of dynamic earth pressure, various analytical methods have been proposed, including those suggested by Seed and Whitman, as well as Wood. Furthermore, subsequent research using experimental methods has been conducted for various types of retaining structures, providing appropriate recommendations for dynamic earth pressure in comparison to the aforementioned methods.

2.1.1 Analytical Methods

The M-O method (Figure 2.1) is derived from the studies conducted by Okabe (1926) and Mononobe & Matsuo (1929) following the great Kanto Earthquake of 1923 in Japan. It was originally developed for gravity walls retaining cohesionless backfill materials and it is the most common approach to determine seismically induced lateral earth pressures on a variety of structures. This method employs a pseudo-static analysis rooted in the Coulomb wedge theory for active and passive earth pressure, along with supplementary vertical and horizontal seismic forces.

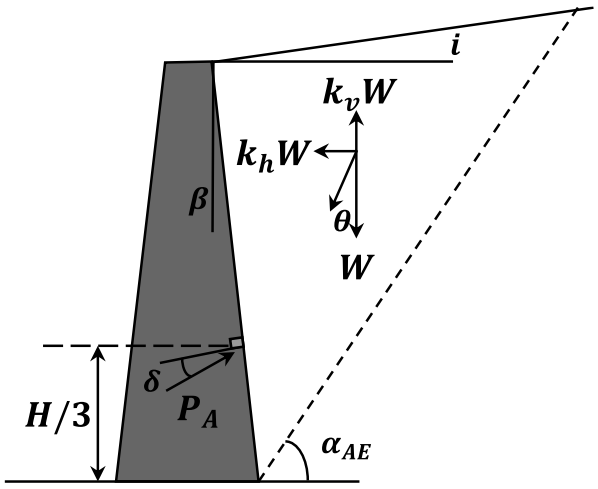

Figure 2.1 Forces considered in the Mononobe-Okabe analysis

Using force equilibrium, the total active thrust P_{AE} per unit length of wall is determined by:

$$P_{AE} = \frac{1}{2}\gamma H^2(1 - k_v)K_{AE} \tag{2.1}$$

$$K_{AE} = \frac{\cos^2(\phi - \theta - \beta)}{\cos\theta \cdot \cos^2\beta \cdot \cos(\delta + \beta + \theta) \cdot \left[1 + \sqrt{\frac{\sin(\phi + \delta) \cdot \sin(\phi - \theta - i)}{\cos(\delta + \beta + \theta) \cdot \cos(i - \beta)}}\right]^2} \tag{2.2}$$

Where, γ = unit weight of the soil

H = height of the wall

ϕ = angle of internal friction of the soil

δ = angle of wall friction

β = slope of the wall relative to the vertical

$\theta = \tan^{-1}(kh/(1-kv))$

kh = horizontal acceleration (in g)

kv = vertical acceleration (in g)

Equation (2.1) describes the total active thrust acting on the wall during seismic loading, and the resulting force is applied at a point located at 1/3H. However, it is crucial to highlight a notable limitation of equation (2.1). It increases exponentially and does not converge if $\theta < \phi - \beta$ (Kramer, 1996), which for typical values of angle of internal friction means accelerations in excess of 0.7 g.

Subsequently, Seed & Whitman (1970) divided the earth pressure induced by earthquakes into static and dynamic components. They asserted that the vertical acceleration component could be neglected due to its insignificance and proposed a simplified equation (Figure 2.2) for the dynamic component.

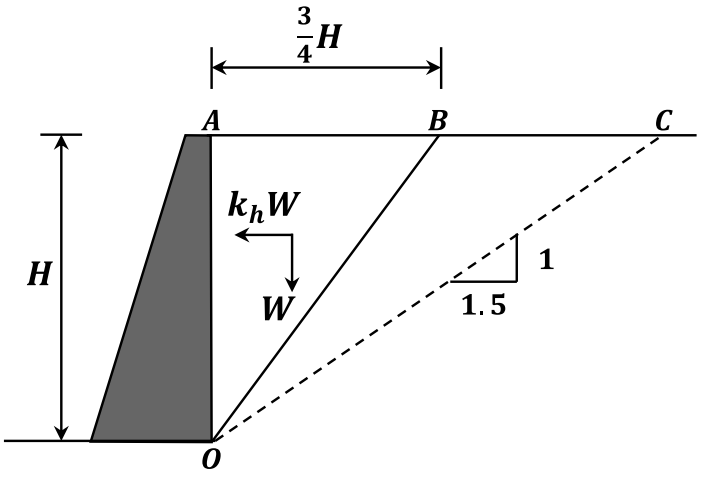

Figure 2.2 Force diagrams used in Seed & Whitman (1970)

they then proposed a simplified expression for the dynamic increment of the active thrust as:

$$P_{AE} = \frac{1}{2} K_A \gamma H^2 + \Delta P_{AE} \tag{2.3}$$

$$\begin{aligned} \Delta P_{AE} &= \mathrm{W_{OAB}} \cdot k_h \\ &= \frac{1}{2} \cdot H \cdot \frac{3}{4} H \cdot \gamma \cdot k_h \\ &= \frac{1}{2} \gamma H^2 \cdot \frac{3}{4} k_h \end{aligned} \tag{2.4}$$

Where, kh is the horizontal ground acceleration (in g)

Moreover, Seed & Whitman (1970) suggest that the resultant of the dynamic force increment should be applied at a height of 0.6H, introducing the concept of the "inverted triangle" to distribute the dynamic force increment. This proposed inverted triangle distribution is based on the experimental study conducted by Matsuo (1941), which served as the basis for suggesting the point of action of dynamic earth pressure at 0.6H.

Wood (1973) proposed seismically induced earth pressures acting on non-yielding walls, such as basement walls. In this case, static earth pressure is determined using the K_0 coefficient, while the dynamic thrust is given by $\Delta P_{AE} = \gamma H^2 A$, with the resultant force acting at a height of 0.6H above the base. The Wood solution assumes a homogeneous linear elastic soil and is applicable when the wall is connected to a rigid base, prohibiting rocking behavior (Figure 2.3).

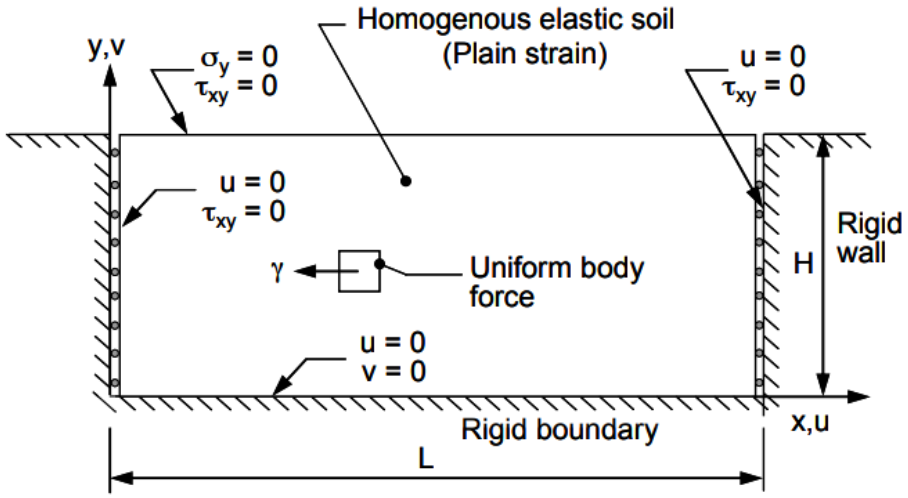

Figure 2.3 Geometry and boundary conditions assumed by Wood (1973)

Various researchers have proposed the distribution and magnitude of dynamic earth pressures using analytical methods. However, the Mononobe-Okabe (M-O) method, which is widely used in domestic and international design standards, is considered overly conservative. However, it should be noted that the target structure of this study, basement walls of buildings, differs from typical retaining structures. The inertial forces of the superstructure can influence the magnitude of dynamic earth pressures acting on basement walls. Therefore, if the superstructure has a large number of stories, the dynamic earth pressures on basement walls could be higher than those predicted by the M-O method. Additionally, there are various conflicting claims regarding the dynamic earth pressure distribution and the point of application. Notably, these proposed distributions and locations were derived under assumptions that

disregarded the influence of the superstructure. Hence, the dynamic earth pressure distribution and the point of application may vary depending on the number of stories in the superstructure.

2.1.2 Experimental Methods

To evaluate the appropriateness of the analytical methods mentioned earlier, various physical modelings were conducted on different types of retaining structures. Researchers such as Al-Atik & Sitar (2010) (Figure 2.4(a)), Candia & Sitar (2013) (Figure 2.4(b)), and Mikola & Sitar (2013) (Figure 2.4(c)) performed a series of centrifuge experiments at the Center for Geotechnical Modeling at UC Davis. By employing different geometries and stiffness, as well as cohesionless and cohesive backfill materials, the researchers modeled a variety of structures, all of which were founded on soil. They concluded that the M-O method was conservative, especially for peak ground acceleration at the surface greater than 0.4 g.

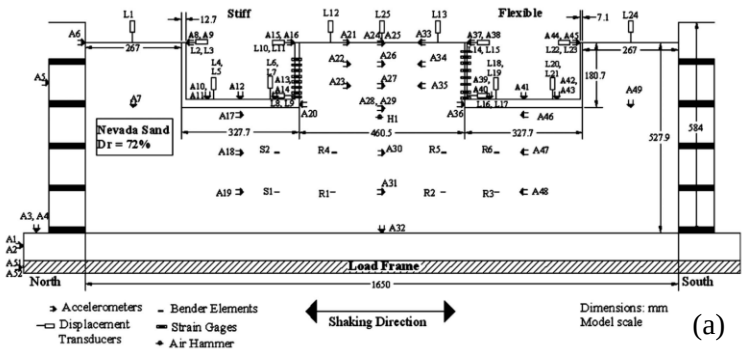

(a)

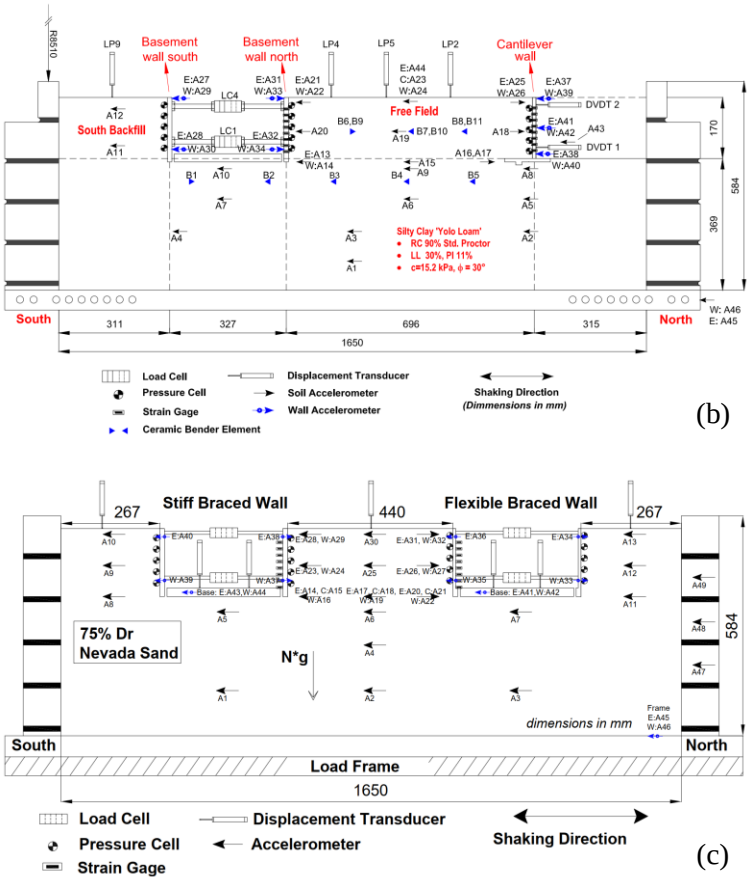

Figure 2.4 Recent dynamic centrifuge experiments: (a) Atik & Sitar (2010), (b) Candia & Sitar (2013) and (c) Mikola & Sitar (2013)

In their study, Mikola & Sitar (2013) investigated the dynamic earth pressure of non-displacing basement, displacing retaining wall, and non-displacing U-shape cantilever wall structures in dry medium-dense sand (Dr-=75%) using both physical modeling and numerical analysis with FLAC2D (Figure 2.4(c)). The seismic earth pressure distribution for all structures exhibited a triangular shape, with the maximum dynamic earth pressure

occurring at the base (Figure 2.5). This finding aligned with the distribution suggested by the Mononobe-Okabe (M-O) method and contradicts the assumption made by Seed & Whitman (1970), which based their approach on the experimental work of Matsuo (1941).

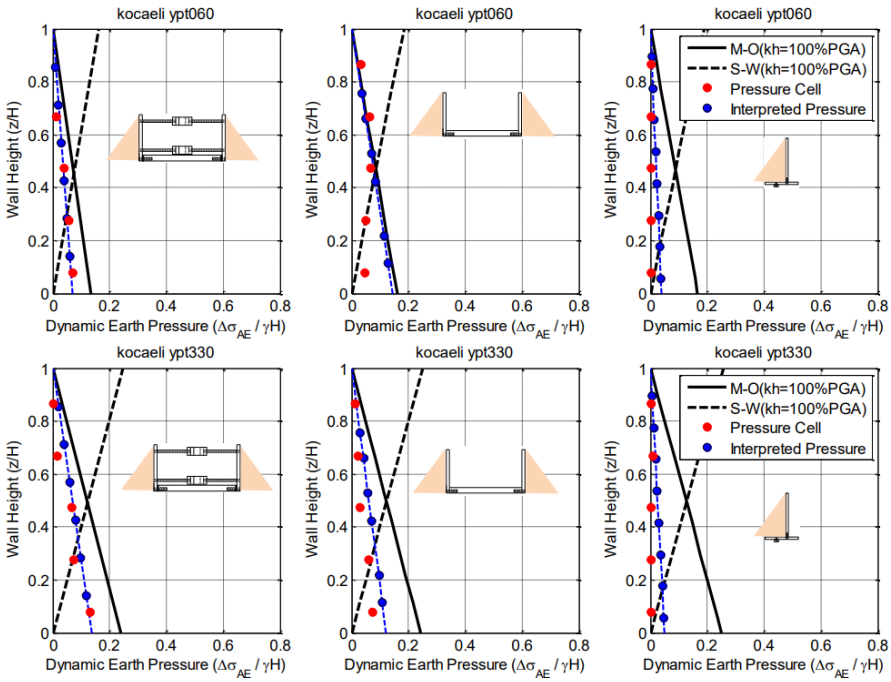

Figure 2.5 Dynamic earth pressure distributions directly measured and interpreted from the pressure sensors and strain gage and load cell data and estimated M-O as well as S-W on walls for KocaeliYPT060-3 (PGA_{ff}=0.25), Kocaeli-YPT330-2 (PGA_{ff}=0.34) by Mikola & Sitar (2013)

Figure 2.6 presents the experimental results regarding the magnitude of seismic earth pressure. It presents the mean and upper bound (UB) for back-calculated values of dynamic earth pressure coefficients for the non-displacing

basement (a), displacing retaining wall (b), as well as non-displacing U-shaped cantilever walls (c), respectively. These coefficients were suggested as a function of the peak ground acceleration (PGA) measured at the top of the soil in the free field. In the case of structures similar to the basement structure studied in this study, as shown in Figure 2.6(a), the Seed & Whitman solution was proposed as an appropriate upper bound suggesting a function for the dynamic earth pressure coefficient with a slope of 0.75 as a function of PGA in the free field.

To summarize, researchers have proposed the magnitude, distribution, and point of application of dynamic earth pressure using analytical methods. These proposals have been further validated through physical modeling experiments conducted under various conditions. However, when it comes to our specific area of interest, which is basement walls of buildings, it is anticipated that the presence of the superstructure and its inertia may have a significant influence on the dynamic earth pressure, particularly as the number of superstructures' stories increases. However, previous studies have focused on structures without considering the superstructure.

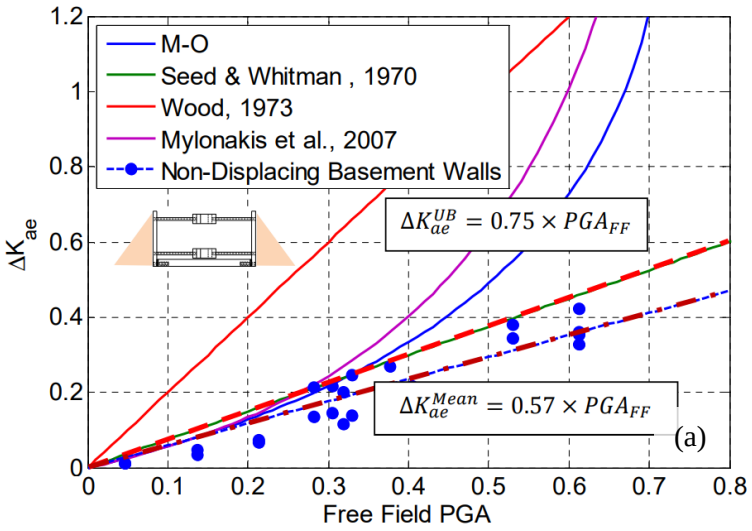
M-O
Seed & Whitman , 1970
Wood, 1973
Mylonakis et al., 2007
Non-Displacing Basement Walls
$\Delta K_{ae}^{UB} = 0.75 \times PGA_{FF}$
$\Delta K_{ae}^{Mean} = 0.57 \times PGA_{FF}$
(a)
ΔK_ae
Free Field PGA

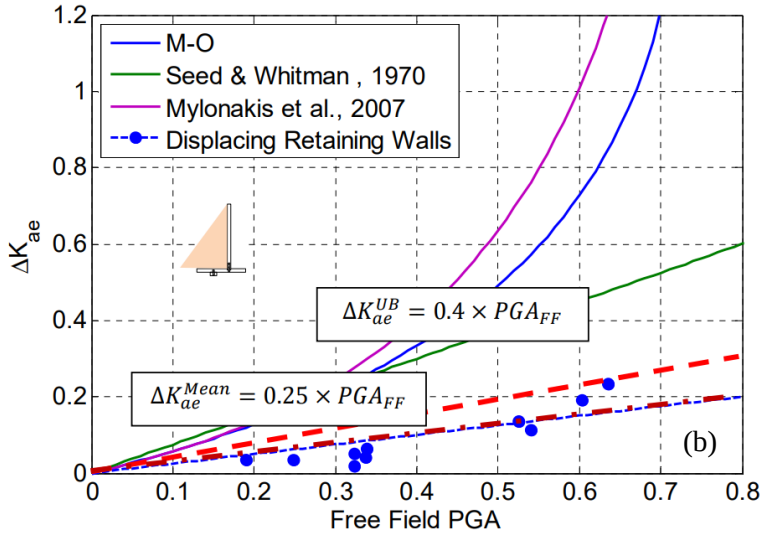
M-O
Seed & Whitman , 1970
Mylonakis et al., 2007
Displacing Retaining Walls
$\Delta K_{ae}^{UB} = 0.4 \times PGA_{FF}$
$\Delta K_{ae}^{Mean} = 0.25 \times PGA_{FF}$
(b)
ΔK_ae
Free Field PGA

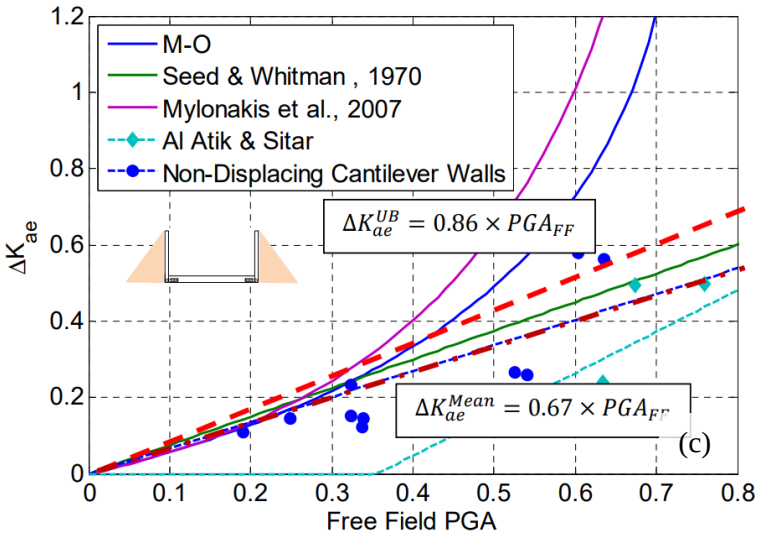

Figure 2.6 Dynamic earth pressure coefficients on (a) the non-displacing basement wall, (b) the displacing retaining wall and (c) the non-displacing U-shaped cantilever wall as function of peak ground acceleration measured at top of soil in free field) by Mikola & Sitar (2013)

2.2 Soil-Structure Interaction (SSI)

As mentioned earlier, in order to accurately predict the response of structures considering the complex interaction between the structure and the soil, a wide range of research has been conducted on Soil-Structure Interaction (SSI). Turan et al. (2013) simplified the superstructure as a single-degree-of-freedom system and performed 1-g shaking table tests with varying numbers of basement floors. The experimental results indicated that the ratio of the effective period of the soil-structure system to that of the structure (T˘/T) decreased for long-period structures and increased for short-period structures as the embedment increased. Hokmabadi et al. (2014) conducted a study on buildings with pile foundations and shallow foundations. Through numerical and physical modeling, they found that the use of pile foundations reduced the

amplification of lateral displacements compared to structures with shallow foundations.

Segalin et al. (2022) presented a study of the Dynamic Soil-Structure Interaction (DSSI) using physical reduced–scale models of a building under different configurations of above-ground and underground stories (Figure 2.7). The researchers proposed that the dynamic effect on lateral soil thrust is primarily influenced by the vibration induced in the superstructure (Figure 2.8). Consequently, inertial interaction plays a crucial role in determining the distribution and magnitude of the lateral thrusts. This finding hold practical significance since the estimation of lateral thrusts typically focuses on soil properties and motion intensity, without considering the characteristics of the superstructure. Therefore, incorporating the dynamic behavior of the superstructure is important for accurate assessment of lateral thrusts.

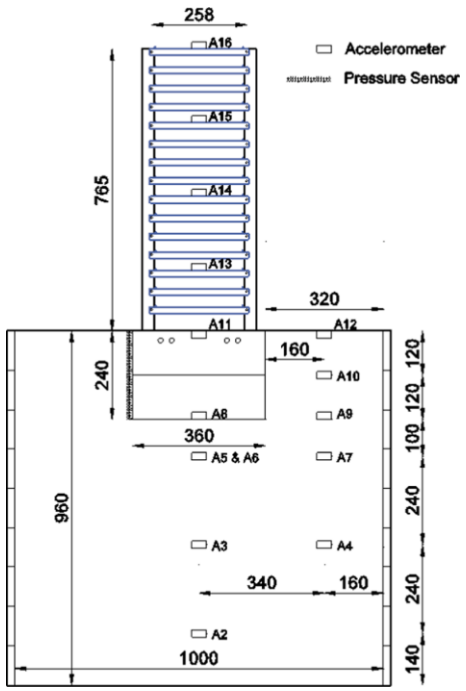

Figure 2.7 Test section and instrumentation by Segaline et al. (2022)

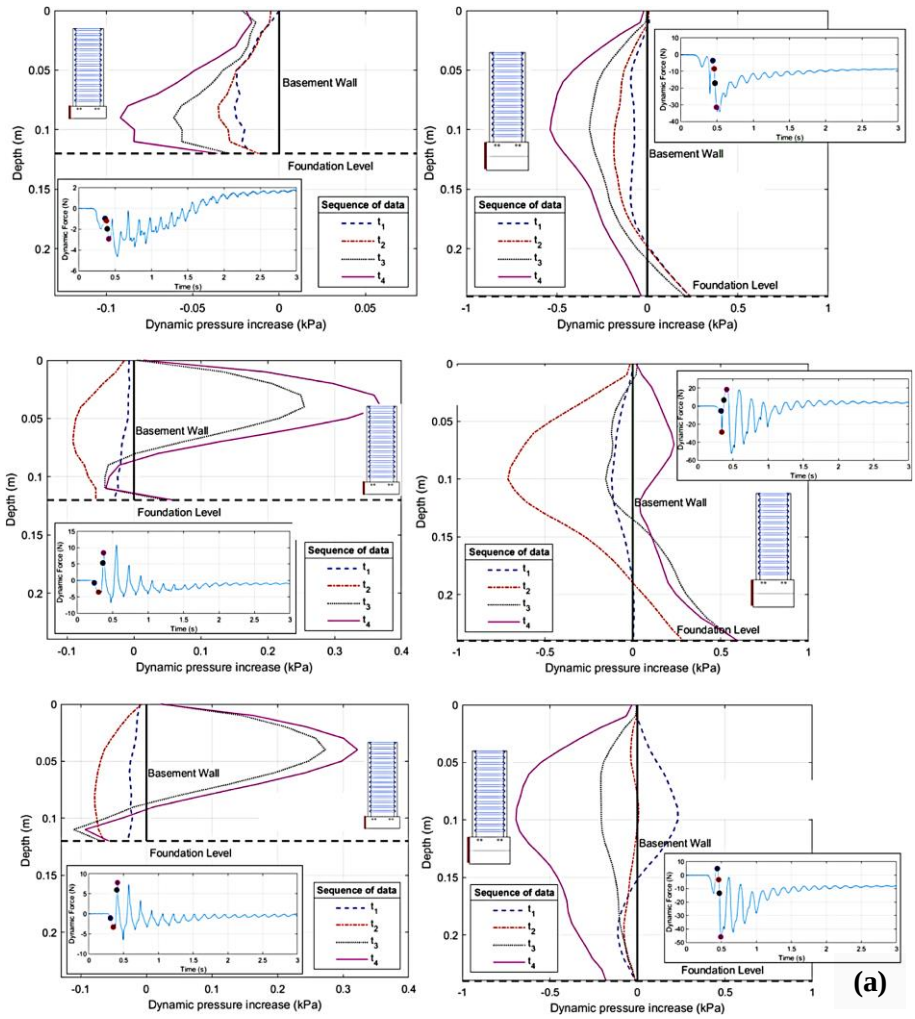
Depth (m)
Dynamic pressure increase (kPa)
Basement Wall
Foundation Level
Sequence of data
t_1
t_2
t_3
t_4
Dynamic Force (N)
Time (s)
(a)

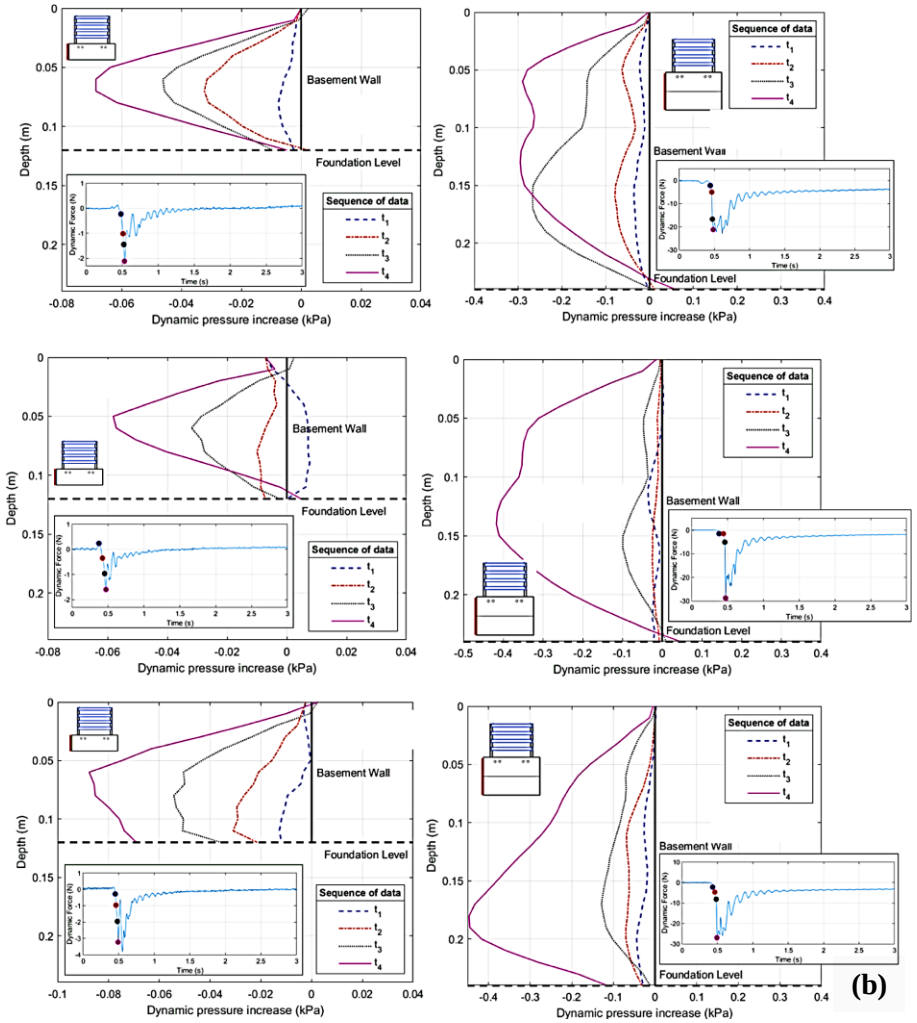

Figure 2.8 Dynamic pressure distribution on walls for (a) high-rise building cases and (b) mid-rise building cases by Segaline et al. (2022)

Recently, there have been numerous studies on the complex interaction between structures and soil. However, there is a lack of experimental research on dynamic earth pressure acting on basement walls of buildings. In a recent study, Segaline et al. (2022) conducted research on the distribution of dynamic earth pressure on these structures using a 1-g shaking table. However,

they only provided a description of the distribution and suggested that the inertia of the superstructure significantly influences the distribution of dynamic earth pressure. Therefore, further comprehensive research is needed to investigate the influence of superstructures on dynamic earth pressure. In particular, it is necessary to determine the trends in dynamic earth pressure distribution based on the number of superstructure stories, considering the various characteristics of seismic waves. Additionally, it is important to evaluate the influence of the number of superstructure stories on the magnitude of dynamic earth pressure by comparing proposed analytical methods like M-O method.

2.3 Summary and Research Gap

The study of dynamic earth pressure acting on retaining structures began with Okabe (1926) and Mononobe & Matsuo (1929) following the Great Kanto Earthquake of 1923 in Japan. Since then, numerous studies have been conducted using analytical methods, focusing on the magnitude, distribution, and point of application of dynamic earth pressure. These studies have also evaluated the appropriateness through experimental methods. Based on these researches, the M-O method that widely used in international seismic design codes for buildings has been suitably and adopted. However, it is important to note that these studies have primarily focused on analyzing the behavior of retaining structures without considering the influence of superstructures. Consequently, caution must be exercised when applying the proposed methods to buildings where the presence of superstructures is expected to significantly impact the dynamic earth pressure in the basement.

On the other hand, with the growing importance of Soil-Structure Interaction (SSI) research, various studies have been conducted to investigate the behavior of basements with superstructures. While research on dynamic

earth pressure is still relatively limited, recent work by Segaline et al. (2022) using a 1-g shaking table experiment has highlighted the significant influence of the inertia forces from the superstructure on the distribution of dynamic earth pressure. However, there is a need for a more detailed analysis of the specific influencing factors and the distribution of dynamic earth pressure considering the number of stories of the superstructure. Furthermore, it is necessary to evaluate and propose suitable approaches by comparing not only the variations in dynamic earth pressure with an increase in the number of floors but also analytical methods, such as the M-O method, as well as experimental research.

The lack of knowledge and research raises motivation for further investigations, especially within the scope of the research work presented in this dissertation, as follows.

- Investigating the influence of dynamic responses of buildings on the seismic earth pressures.
- Effect of the presence and stories of superstructure on the seismic earth pressure distribution.
- Effect of the presence and stories of superstructure on magnitude of the seismic earth pressure.
- Evaluation and formula proposal for the magnitude of dynamic earth pressure according to the number of layers of the superstructure

Chapter 3 Physical Modeling

3.1 Introduction

In this study, experimental research was conducted on the dynamic earth pressure acting on basement walls of buildings using a 1-g shaking table. In section 2, an overview of equipment used will be provided, including the shaking table and soil box, and introduced a preliminary test on the boundary effects of the rigid box. To analyze the prototype behavior, it is crucial to simulate a model that closely resembles the prototype characteristics. The model structure will be divided into the superstructure and basement, focusing on the characteristics that were considered in this study. The numerical analysis and preliminary test conducted to simulate the natural frequency of the superstructures will be emphasized. The measuring instruments used and their purposes will be described in the measuring instrument section. Furthermore, the process of obtaining modified forces through a dynamic earth pressure measuring system in this experiment will be explained. The soil characterization section will present the particle size distribution and soil properties. Model construction discusses the sequential process of constructing the test section. Lastly, the test program will introduce the ground conditions and input seismic waves, along with presenting the experimental cases and representative layout of 1-g shaking table test showing the positions of measuring instrument and physical model.

3.2 1-g Shaking Table Test Setup

3.2.1 Equipment

Figure 3.1 provides perspective views of 1-g shaking table and rigid soil box. The 1-g shaking table is an experimental device used to study the behavior of structures under dynamic loads. The shaking table used in this study has a control frequency range of up to 80Hz, a control maximum stroke of ± 50 mm, a maximum acceleration of 1g, and a maximum specimen weight of 5 tons. The rigid soil box has dimensions of 200cm x 50cm x 70cm (length x width x height). It was specifically designed with acrylic material to facilitate observation of the test section during the model construction and testing processes.

Figure 3.1 Perspective views of 1-g shaking table and rigid box

The rigid box used in this study restricts the lateral displacement of the model soil within the soil box. Moreover, the stiffness of the walls can cause the generation of reflected waves that interfere with the horizontal behavior of the soil. To investigate the influence of the boundary effect, a preliminary test

was conducted. Figure 3.2 depicts the test section and instrumentation of the preliminary test. To mitigate the boundary effect of the rigid box, a commonly used 5cm sponge material was attached to the walls (Yang et al., 2010). Using the measured acceleration at point A as the input motion, accelerometers were used to measure the acceleration at points B, C, D in the middle of the soil and points E, F, G on the surface. Subsequently, the Peak Ground Acceleration (PGA) and Amplitude Factor (AF) were employed to evaluate the effectiveness of the 5cm sponge in reducing the boundary effect of the rigid soil box.

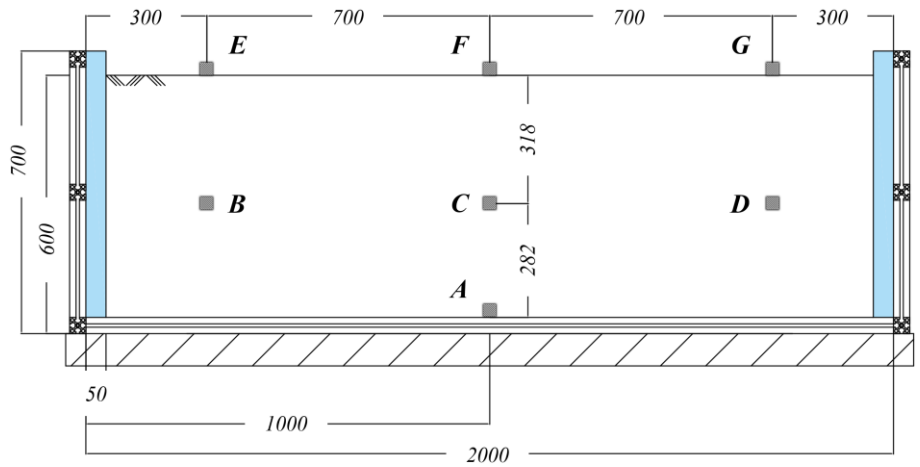

Figure 3.2 Test section and instrumentation for boundary effect preliminary test

Points A, C, and F located at the center of the soil box were considered free-field motion. Subsequently, the acceleration results at points B, D, E, and G, located away from the center, were compared with the corresponding free-field motion at the same height. For the purpose of comparison, two different seismic waves were utilized: the Loma Prieta 1989 earthquake, which encompassed a wide range of frequencies (PGA=0.23g), and a 15Hz sine wave

(PGA=0.15g).

Figure 3.3 represents the results of the Loma Prieta 1989 earthquake at -0.318m depth. In (a), the acceleration time histories are presented. The PGA of 0.26g was measured consistently across all locations, and it was observed that the waveforms were also highly similar, regardless of the position. In (b), the fast Fourier transform (FFT) is shown, revealing that locations B, C, and D exhibit remarkably similar results across all frequency ranges. Figure 3.4 represents the surface (0m) response to the same seismic wave. In the acceleration time history (a), slightly higher PGA values are observed at location G compared to location F, which is attributed to the reflection waves generated by the walls of the soil box in the shaking direction. The FFT results (b) demonstrate a high degree of similarity in the dominant frequency range across all locations, with minor discrepancies beyond approximately 40Hz. Figure 3.5 depicts the results of a sine wave at a depth of -0.318m. In (a), the acceleration time history shows a consistent PGA magnitude at all locations. The FFT analysis (b) indicates similar amplitudes at the input motion's frequency component of 15Hz. Figure 3.6 represents the surface (0m) response reflecting the same findings as depicted in Figure 3.5.

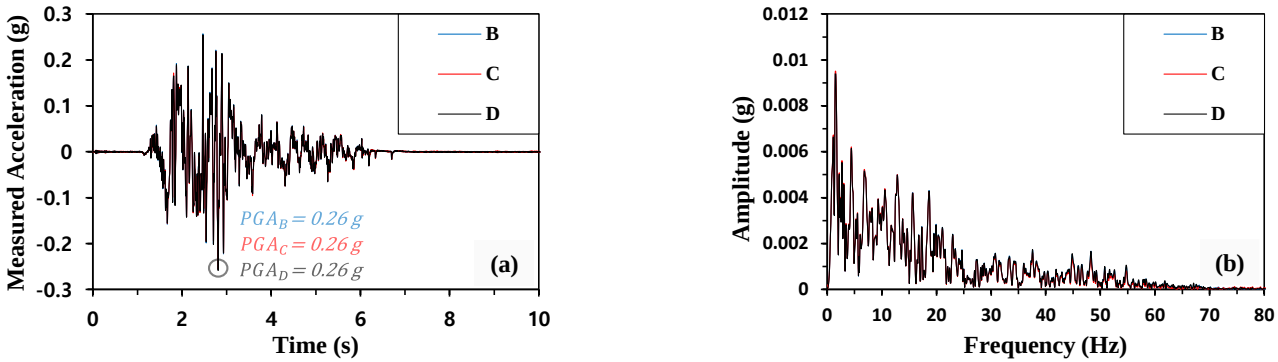

Figure 3.3 Test results for the Loma Prieta 1989 (a) acceleration time history and (b) fast Fourier transform at -0.318m

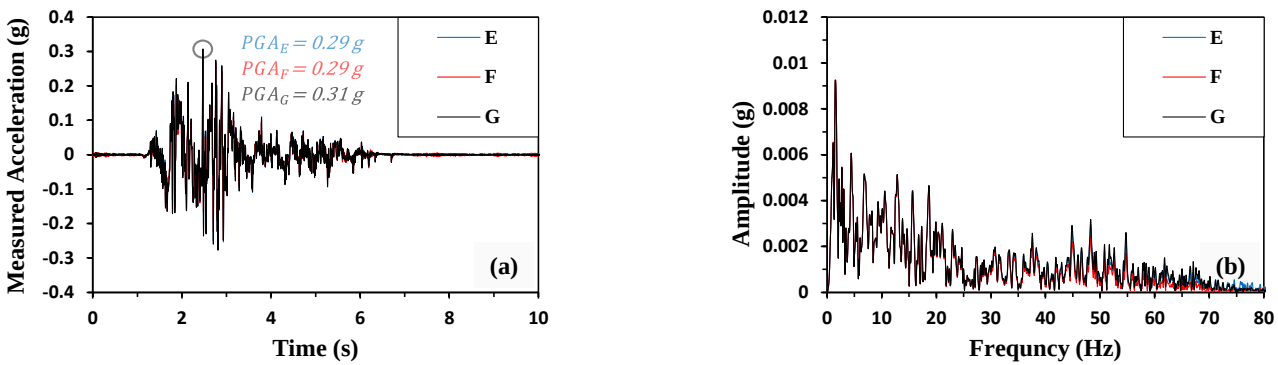

Figure 3.4 Test results for the Loma Prieta 1989 (a) acceleration time history and (b) fast Fourier transform at 0m

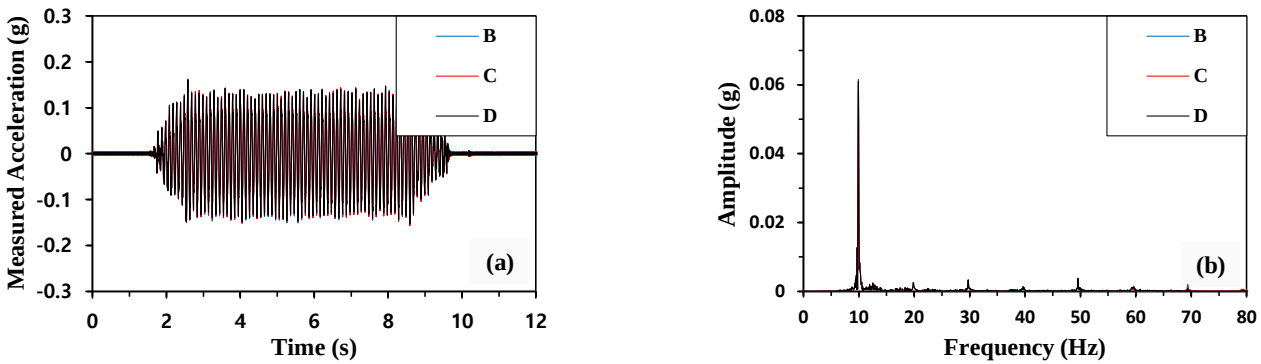

Figure 3.5 Test results for the sine wave (a) acceleration time history and (b) fast Fourier transform at -0.318m

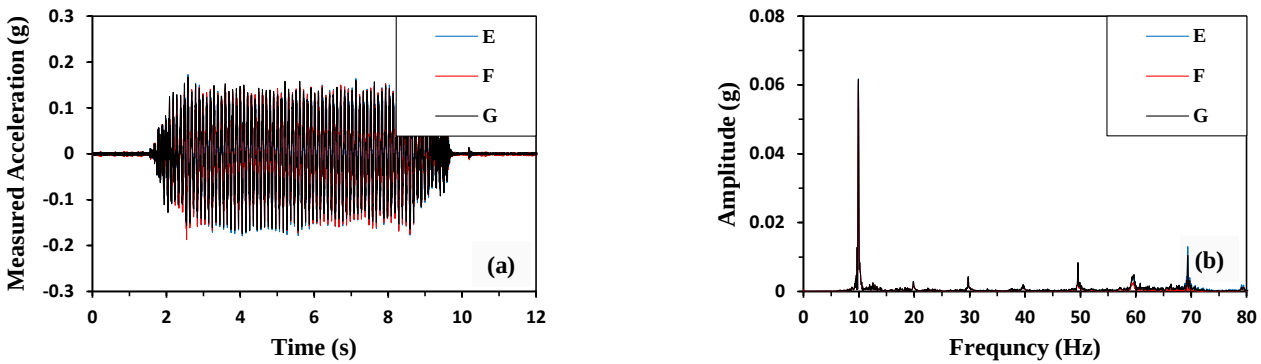

Figure 3.6 Test results for the sine wave (a) acceleration time history and (b) fast Fourier transform at 0m

The effective assessment of the boundary effect can be achieved by utilizing the Amplification Factor (AF) in conjunction with PGA. The AF was determined by dividing the peak horizontal ground acceleration at the ground surface (0m) and at a depth of -0.318m by the peak horizontal ground acceleration obtained from the Loma Prieta 1989 earthquake acceleration history ($\mathrm{PGA_{input}} = 0.23g$) and the sine wave ($\mathrm{PGA_{input}} = 0.15g$), respectively.

$$\mathrm{AF} = \frac{PGA}{PGA_{input}} \tag{3.0}$$

Where, PGA is the peak ground acceleration of the point of interest for amplification and PGA_{input} is the peak ground acceleration of the input motion.

Table 3.1 presents the amplification factor (AF) at each location for the LomaPrieta 1989 earthquake. Comparing the free-field locations C with B, and D at -0.318m, a high degree of similarity can be observed. At the ground surface (0m), all locations exhibit larger values compared to the middle location, indicating amplification due to the seismic wave. Locations E and G show slightly higher values than the free-field location F, indicating a slight influence from the reflected waves generated by the rigid wall where the seismic load is applied. Table 3.2 represents the results for the sine wave. Similar to the LomaPrieta 1989 earthquake, amplification occurs at the ground surface (0m), showing slightly higher values than the middle location (-0.138m). However, regardless of the location, consistent values comparable to the AF of the free-field can be observed at the same height. Therefore, the preliminary test performed to investigate the influence of the boundary effect concluded that the

attachment of 5cm sponge to the wall effectively mitigates the boundary effect in the rigid box.

Table 3.1 Comparison of amplification factors (AF) by location by LomaPrieta 1989 earthquake ($\mathrm{PGA}_{\mathrm{input}} = 0.23g$)

Name	Location	PGA (g)	AF
A	Bottom (-0.6m)	0.23	1.00
B		0.26	1.10
C	Middle (-0.318m)	0.26	1.10
D		0.26	1.11
E		0.29	1.26
F	Surface (0m)	0.29	1.24
G		0.31	1.32

Table 3.2 Comparison of amplification factors (AF) by location by sine wave ($\mathrm{PGA}_{\mathrm{input}} = 0.15g$)

Name	Location	PGA (g)	AF
A	Bottom (-0.6m)	0.15	1.00
B		0.16	1.07
C	Middle (-0.318m)	0.16	1.04
D		0.16	1.05
E		0.18	1.17
F	Surface (0m)	0.19	1.22
G		0.18	1.18

3.2.2 Model Structure

The prototype of this experimental model follows the superstructures and basements provided by the architectural structure guidelines of the SH (2019).

To analyze the behavior of the prototype through model testing, it is crucial to accurately replicate the characteristics of the structural model. This requires establishing appropriate scaling relationships between the model and the prototype. Iai (1989) proposed a similitude law that incorporates governing equations considering the equilibrium, constitutive law, and strain definition of the soil-structure-fluid system. Furthermore, many studies on soil-structure interaction (SSI) based on physical modeling using shaking tables have been developed using this similitude law (Segaline et al., 2022). The scaling relationships employed in this study are summarized in Table 3.3.

Table 3.3 Scaling factors in this study (Iai, 1989)

Length	λ	Mass	λ^3	Time	$\lambda^{\frac{1}{2}}$
Force	λ^3	Mass density	1	Frequency	$\lambda^{-\frac{1}{2}}$
Stiffness	λ^2	Acceleration	1	Shear wave velocity	$\lambda^{\frac{1}{2}}$
Stress	λ	Strain	1	Modulus	λ

In small-scale modeling, the prototype and the model are connected through scaling factors. These factors represent the ratio between corresponding physical properties of the prototype and the model, such as length or material modulus. However, due to small-scale restrictions, it is usually impossible to simultaneously comply with all the scaling factors. For this reason, depending on the model objective, only the relevant physical properties shall be properly scaled.

In this study, the superstructure was scaled using polyethylene (PE) material to match the prototype's natural frequencies, length, and mass. The

natural frequencies of the structure have a significant influence on its dynamic behavior and are closely related to the frequencies of seismic waves. The height of the structure is a factor influenced by its natural frequencies. Mass is another crucial characteristic as it not only affects the natural frequencies but also contributes to the inertial forces of the superstructure. The physical model of the superstructure adheres to the guidelines provided by SH (2019). The guidelines provide the height of the building and specify the dimensions of each component, indicating the use of reinforced concrete. Therefore, by calculating the unit weight of reinforced concrete, it was possible to accurately replicate the height and mass of the superstructure in the model. However, since there is no specific prototype building available, determining the natural frequencies for the prototype required a series of steps and procedures.

This study investigates the influence of superstructure height on dynamic earth pressure. Thus, the structure employed in the experiment consists of a combination of 3-story basement and superstructures with 0 (BO), 3 (LB), and 9 (HB) floors (Table 3.4). Furthermore, while there are various types of structures available to resist seismic loads, this study adopts concrete moment-resisting frames.

Table 3.4 Target buildings of this study with various upper floors

No.	Name	Superstructure	Basement
1	Basement Only (**BO**)	0-story	3-story
2	Low-rise building with Basements (**LB**)	3-story	
3	High-rise building with Basements (**HB**)	9-story	

To determine the appropriate natural frequency of the prototype structure, the ETABS software was utilized. It was then compared with the approximate formulas proposed by ASCE (2016) and MOLIT (2019). ETABS is a specialized engineering software used for the analysis and design of multi-

story buildings. Additionally, Figure 3.7 represents a schematic diagram of a prototype structure simulated using ETABS.

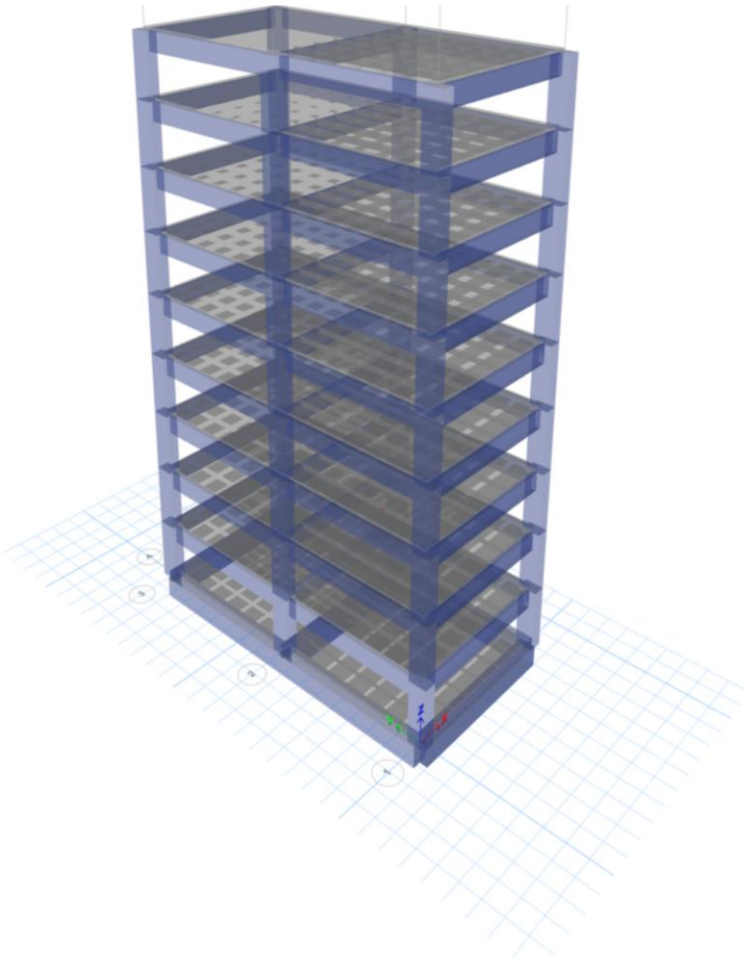

Figure 3.7 Modeling for structural natural frequencies using ETABS

The approximate formula is as follows,

$$T_a = C_t h_n^x \tag{3.0}$$

where, h_n = The structural height

C_t and x are determined from Table 3.5

Table 3.5 Values of Approximate Period Parameters C_t and x

Structure Type	C_t	x
Moment-resisting frame systems in which the frames resist 100% of the required seismic force and are not enclosed or adjoined by components that are more rigid and will prevent the frames from deflecting where subjected to seismic forces:		
Steel moment-resisting frames	0.0724	0.8
Concrete moment-resisting frames	0.0466	0.9
Steel eccentrically braced fames	0.0731	0.75
Steel buckling-restrained braced frames	0.0731	0.75
All other structural systems	0.0488	0.75

When comparing the values obtained from the ETABS analysis and the approximate formulas, it was determined that the determined natural frequencies of the prototype structures for LB and HB were reasonable (Table 3.6).

Table 3.6 Comparison of natural frequency of ETABS and approximate Formula

Case	Natural frequency (Hz)	
	ETABS (Numerical analysis result)	Approximate formula (from ASCE, 2016)
LB	3.17	2.89
HB	1.18	1.07

To verify whether the natural frequencies of the physical model match well with the scaled natural frequencies obtained from the prototype, a sweep test was conducted. The structure was connected to a shaking table under fixed conditions for the sweep test. By installing accelerometers at each floor, the occurrence of resonance phenomenon in the structure at specific vibration frequencies was confirmed (Figure 3.8).

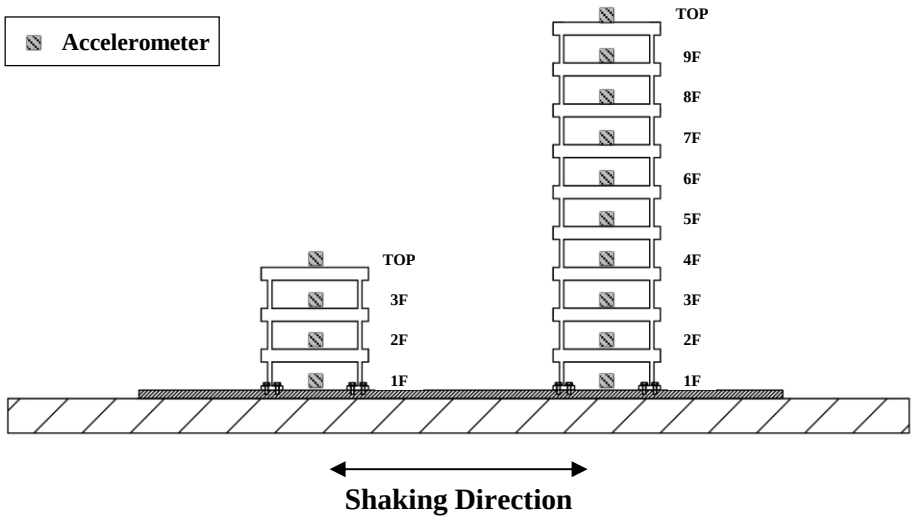

Figure 3.8 Test section and instrumentation for sweep test

The sweep wave is a seismic wave characterized by a constant amplitude and a changing frequency over time. Figure 3.9 represents the sweep wave used in the sweep test, with an amplitude of 0.10g (a) and a frequency range of 1-60Hz (b). The target natural frequency for LB was 18.24Hz, and the sweep test resulted in a frequency of 22.26Hz. For HB, the target natural frequency was 6.77Hz, and the sweep test yielded a frequency of 6.39Hz (Figure 3.10). Hence, the physical models produced through the sweep test accurately replicated the desired natural frequencies of the prototypes.

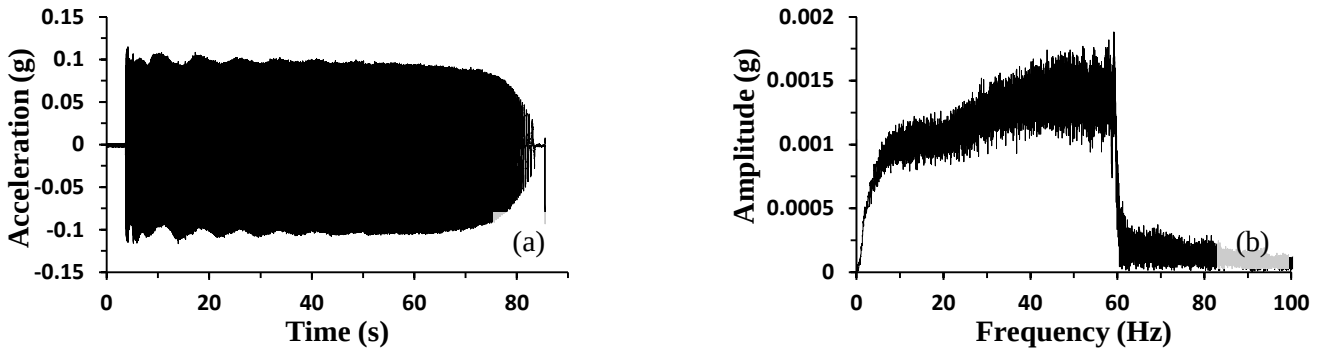

Figure 3.9 sweep wave (a) acceleration time history and (b) fast Fourier transform for structural natural frequencies

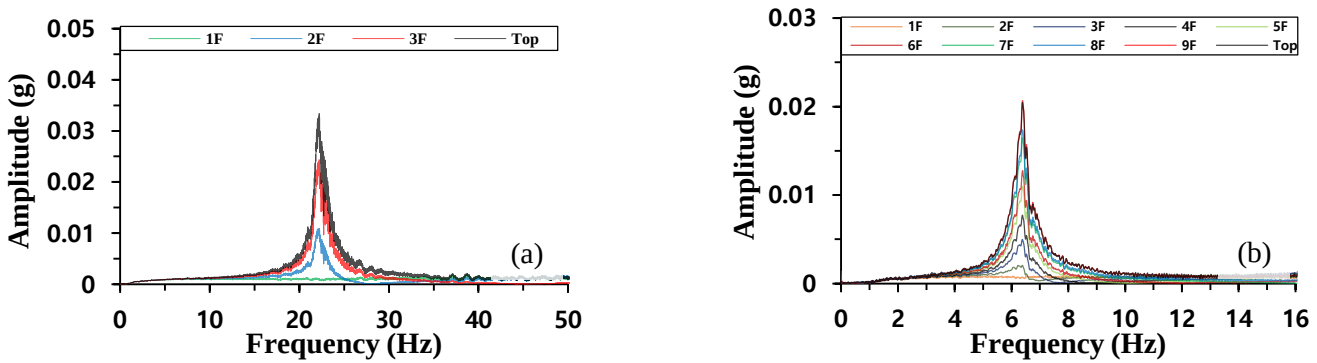

Figure 3.10 Fast Fourier transform results of acceleration measured at each layer of the structure (a) LB and (b) HB

The basements were made using aluminum to obtain rigidity compared to the soil and superstructure and were scaled in terms of mass and length. Figure 3.11 provides schematic views of the physical models used in the experiment. Table 3.7 comprehensively presents the scaling relationship of the physical models, which has been validated through numerical analysis and the sweep test.

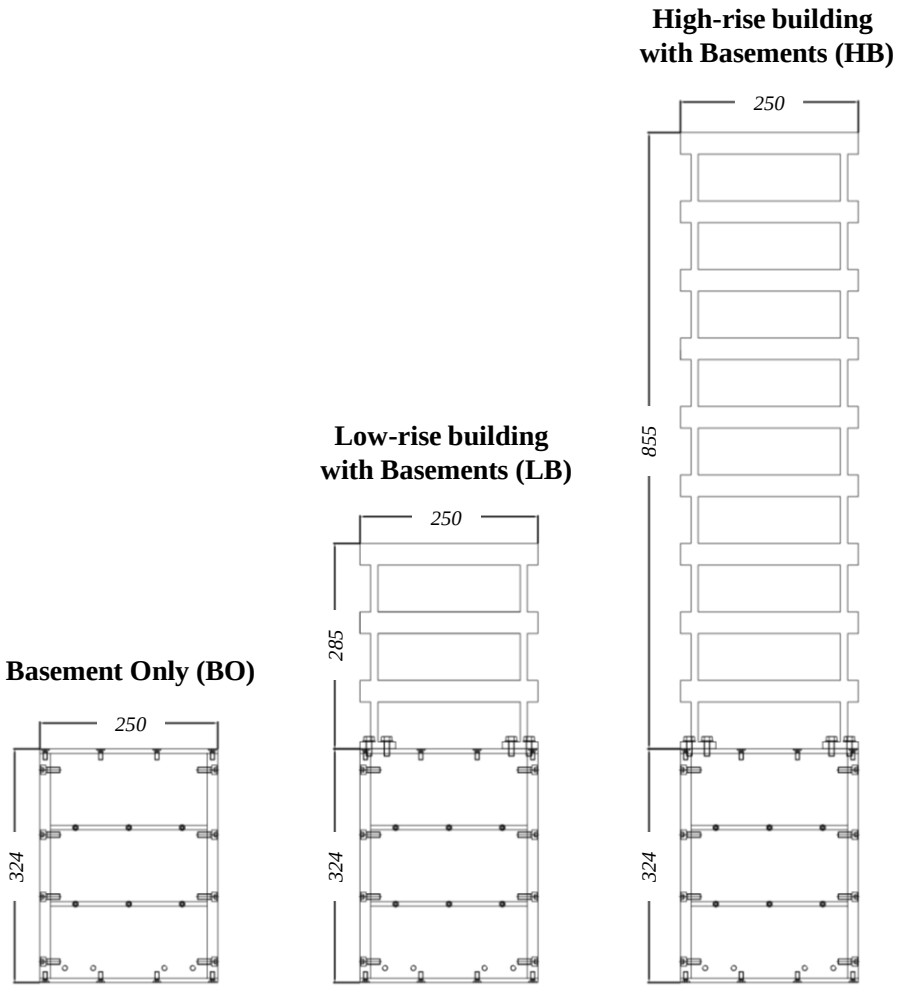

Figure 3.11 Schematic views of physical Models (dimensions in mm)

Table 3.7 Scaling relationship for λ=33

Case	Superstructure							Basement			
	Natural frequency (Hz)			Height (m)		Mass (kg)		Height (m)		Mass (kg)	
	Prototype	Model (target)	Model (empirical)	Prototype	Model	Prototype	Model	Prototype	Model	Prototype	Model
BO	-	-	-	-	-	-	-				
LB	3.17	18.24	22.26	9.30	0.29	402773	10.99	10.80	10.69	872320	25.23
HB	1.18	6.77	6.39	27.90	0.86	1208318	32.96				

3.2.3 Measuring Instrument

Measuring instruments used in this study are accelerometers, LVDTs and loadcells. The accelerometers were ARH-10A from TML (Figure 3.12 (a)) with a capacity of $10m/s^2$. these were used to measure the acceleration of the soil and superstructure. In particular, acceleration results installed on the top of superstructure were used to analyze the influence of the superstructure's inertial forces on the dynamic soil pressure acting on the basement (Figure 3.12 (b)). The accelerometers located in the soil were positioned using an acrylic plate, allowing them to move along with the soil during shaking. Additionally, these were placed on load cell plates. To measure the pure dynamic soil pressure acting on the ground, it is necessary to obtain the modified force by eliminating the inertial forces of the pressure plate. This process is a crucial procedure, and further details will be provided in the paragraph explaining the load cells.

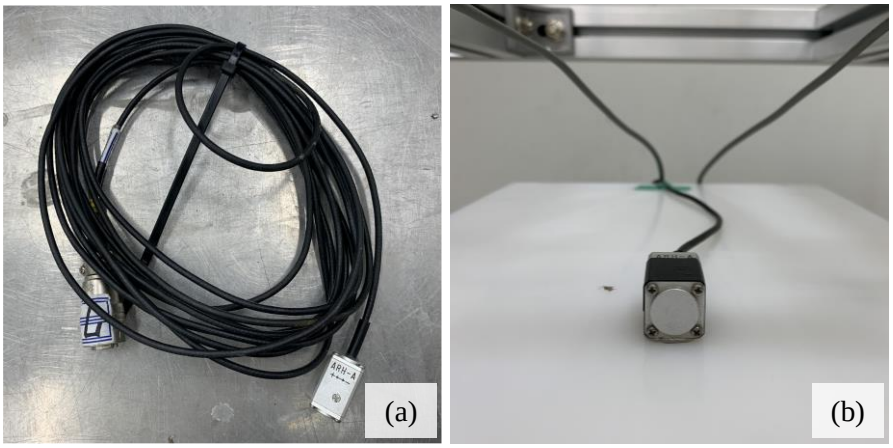

Figure 3.12 Set-up of accelerometers

The LVDTs shown in Figure 3.13(a) are KDC from RADIANQBio with a capacity of 100-300mm. The LVDTs were installed to measure the horizontal and vertical displacements of the structure caused by seismic loads (Figure 3.13(b)). The LVDT installed in the vertical direction in the soil was used to measure the settlement of the ground.

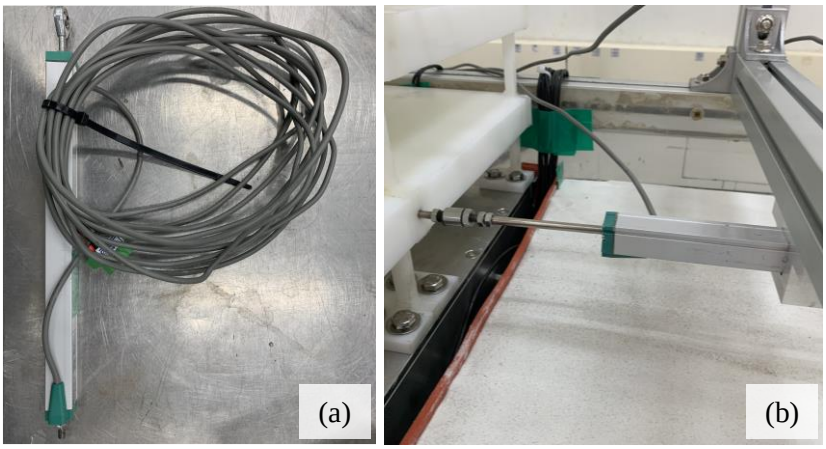

Figure 3.13 Set-up of LVDTs

The loadcells, as shown in Figure 3.14(a), are CBF30 loadcells from CASKOREA with a capacity of 20kgf. In Figure 3.14(b), the loadcells are installed on the sides of the basement to measure the dynamic earth pressure. The basement consists of 3 floors, and two loadcells are installed on each floor. The loadcells measure the tensile and compressive forces acting on the central rod. One side of the loadcell is attached to the exterior wall of the basement, while the other side is bolted to the loadcell plate. The dynamic earth pressure measuring system (Figure 3.15) has been constructed in this configuration, allowing for precise measurement of the forces acting on the loadcell plate from the surrounding soil.

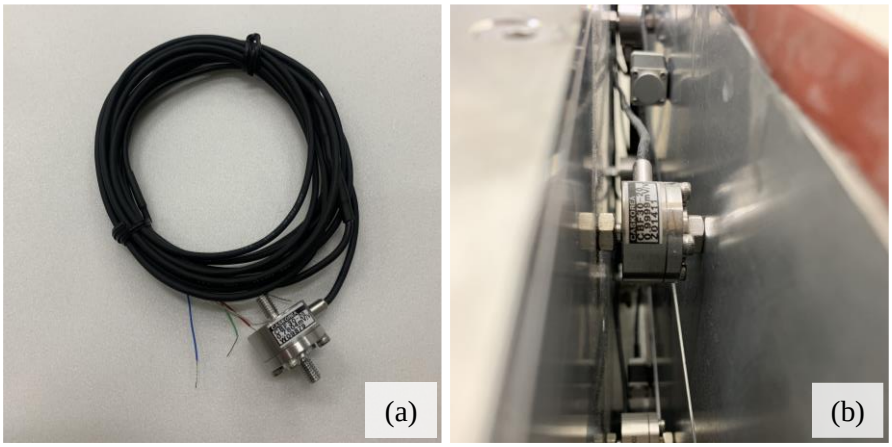

Figure 3.14 Installation of loadcells

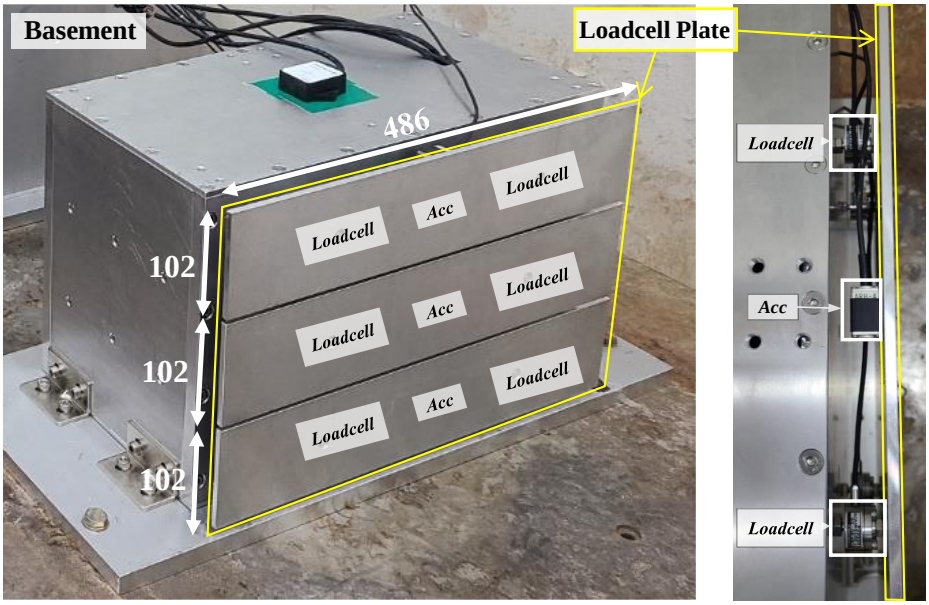

Figure 3.15 Dynamic earth pressure measuring system

By utilizing this system, it is possible to measure dynamic earth pressure reasonably through loadcells. However, a challenge arises as the measured force on the loadcell includes not only the soil pressure exerted from

the ground but also the inertial force of the loadcell plate. To address this issue, a preliminary test was conducted using the Loma Prieta 1989 earthquake, which contains various frequency components.

Initially, the measured force, obtained by adding the two loadcell measurements, was compared to the inertial force derived by multiplying the mass and acceleration of the loadcell plate (Figure 3.16(a)). When zoomed in on the raw data, it was observed that the two forces exhibited peaks at different time intervals (Figure 3.16(b)). To address this, an offset process was performed as the first step in modifying the force.

The resulting time history after the offset process is shown in Figure 3.17(a). When zoomed in around 4.91 s, it was noticed that the time histories aligned but the inertial force was smaller than the measured force (Figure 3.17(b)). This was resolved by applying mass correction to scale up the inertial force. Figure 3.18(a) shows the force time history after mass correction. Upon closer examination around 4.91 s (Figure 3.18(b)), it was observed that the inertial force and measured force exhibited similar waveforms. Initially, the difference between the inertial force and measured force ranged from 0.6 to 0.8 N, but after the modified force process, this difference was reduced by 75-80% to a range of 0.1-0.2 N (Table 3.8).

Therefore, by appropriately removing the inertial force of the loadcell plate, the main experiment was able to measure only the dynamic earth pressure exerted by the soil.

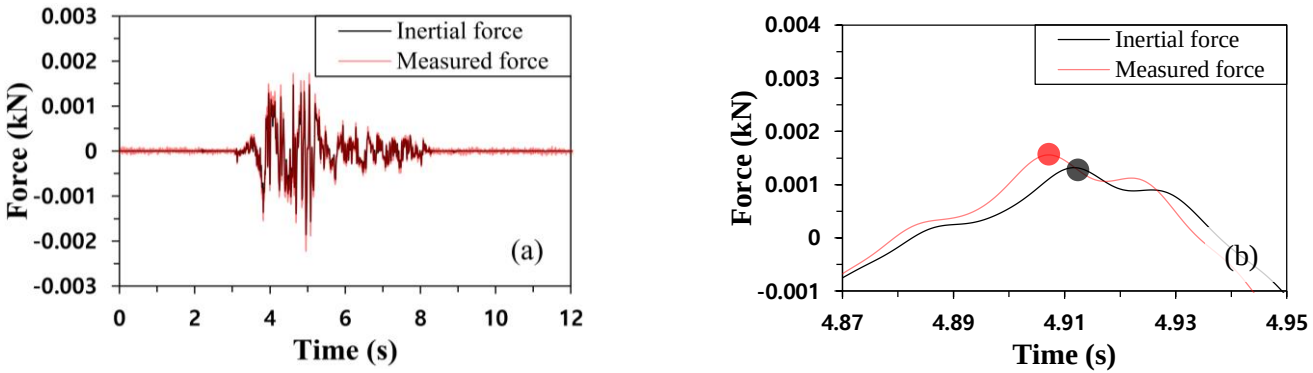

Figure 3.16 Raw data before modified force (a) force time history (b) different peaks at around 4.91 s

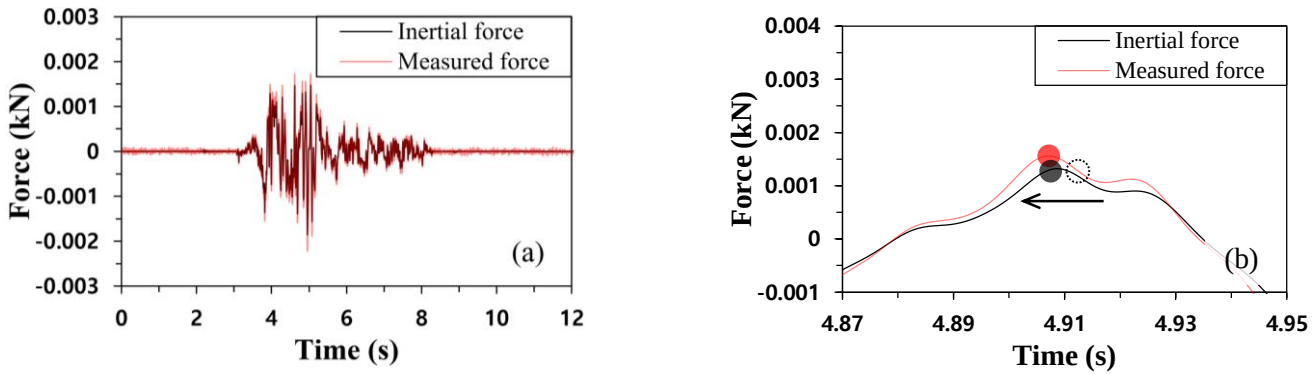

Figure 3.17 Time correction through offset process (a) force time history (b) different peaks at about 4.91 s

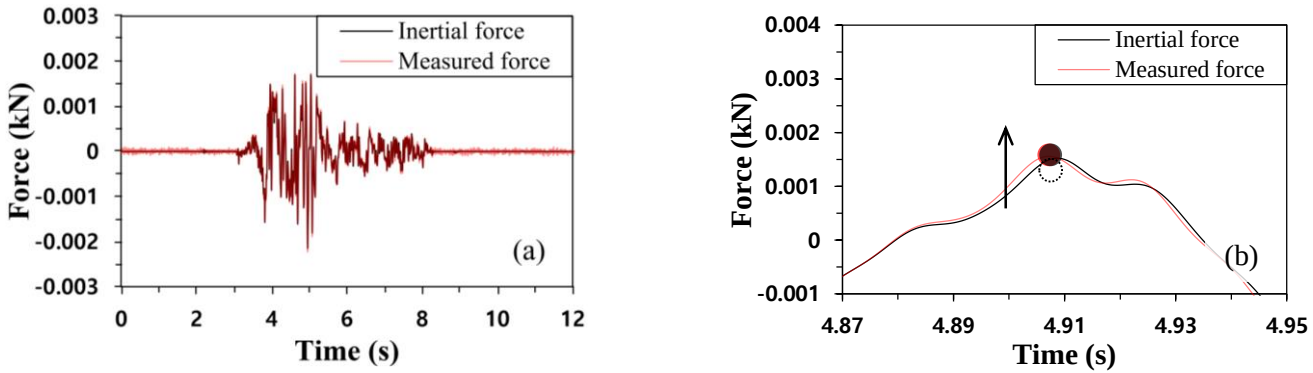

Figure 3.18 Mass correction with additional mass (a) force time history (b) two similar peaks at about 4.91 s

Table 3.8 Comparison of maximum difference between internal force and measured force before and after modification and reduction rate

Location	Max. difference between inertial force and measured force (N)			Reduction rate (%)
	Raw	Offset	Additional mass	
1B	0.772	0.411	0.192	75
2B	0.630	0.341	0.126	80
3B	0.715	0.369	0.181	75

3.2.4 Soil Characterization

The material used in this study was poorly graded sand, specifically silica sand. The grain size distribution and physical properties of the silica sand can be observed in Figure 3.19 and Table 3.9, respectively. Since a specific prototype soil was not determined, an arbitrary cohesionless soil condition was implemented for the main experiment.

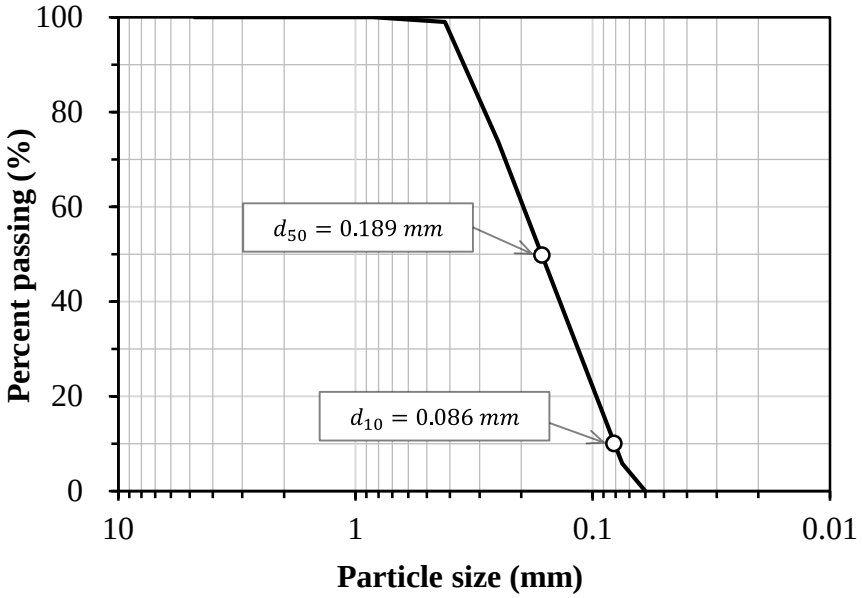

Figure 3.19 Grain size distribution curve of silica sand

Table 3.9 Physical properties of silica sand

Properties	Values
Specific gravity	2.65
Coefficient of uniformity, C_u	2.50
Maximum dry unit weight, (kN/m^3)	17.16
Minimum dry unit weight, (kN/m^3)	12.65
Soil classification (USCS)	SP

3.2.5 Model Construction

The experimental model was constructed as following procedures (Figure 3.20).

① The foundation soil is divided into three layers (10/10/8.2cm) and silica sand is added to each layer based on the required weight for a relative density of 80.6% (γ_d = 16.05kN/m3). The soil is then compacted for 10 minutes using a sine wave with a frequency of 20Hz and an amplitude of 0.6g.

② After the foundation soil is compacted to a height of 0.282mm, the basement, equipped with the accelerometers and loadcells, is placed.

③ The basement has a 7mm gap in the width direction, both in front and behind, to prevent wall friction with the soil box. OHP film is used to seal these gaps to prevent the entry of soil.

④ The adjacent soil is divided into three layers of 11.8/10/10cm, and each layer is filled with soil corresponding to Dr 80.6% (γ_d = 16.05kN/m^3). The soil is compacted for 10 minutes to achieve compaction.

⑤ In cases where there are superstructures (LB, HB), the superstructure

is combined with the basement by bolting.

⑥ The accelerometers located in the ground are positioned using acrylic plates during ground composition, while the accelerometers and LVDTs on the structure and ground surface are installed.

⑦ All measurement devices are connected to the data logger and their status is checked.

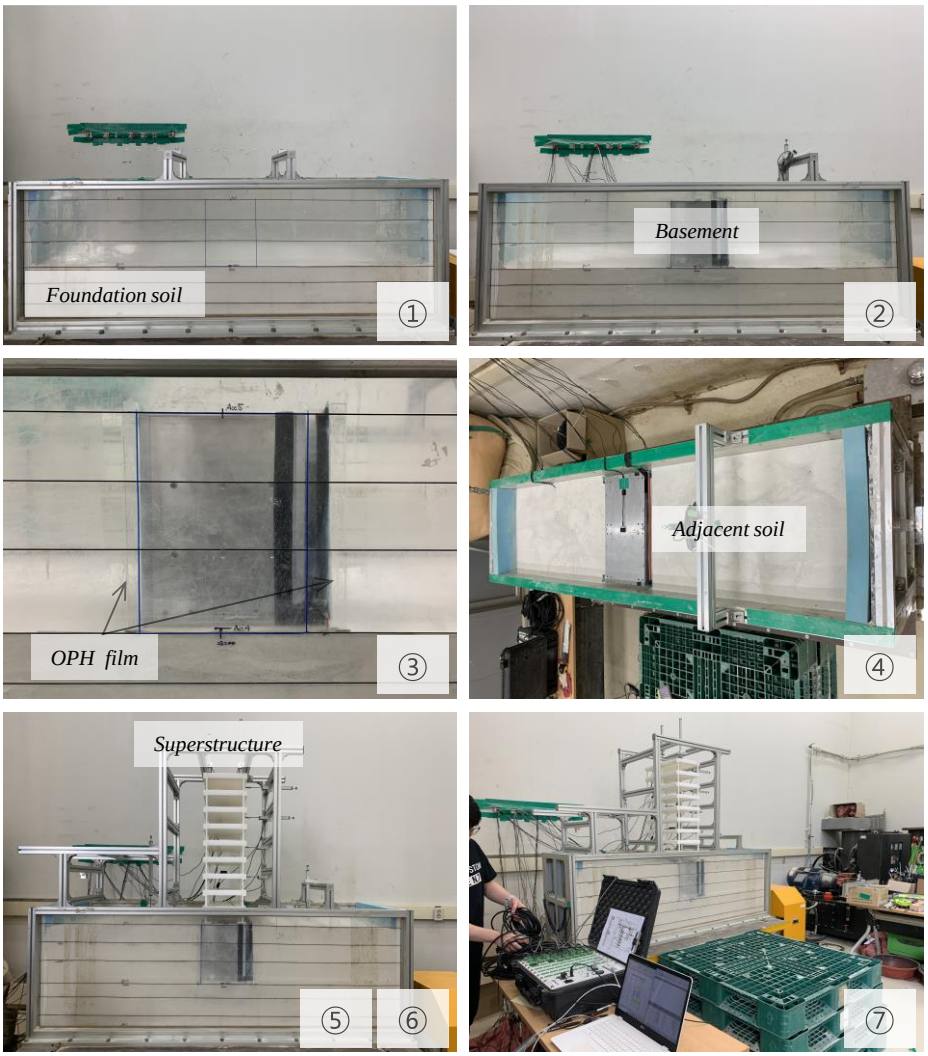

Figure 3.20 Procedure of construction for physical modeling

3.2.6 Test Program

This study aims to investigate the relationship between dynamic soil pressure and the number of stories in the superstructure, which is influenced by the characteristics of input seismic waves. Therefore, different vibration frequency components (3, 5, 6Hz) and various amplitudes (0.10, 0.15, 0.20, 0.30g) of seismic waves were used. Figure 3.21 provides an example of the applied seismic waves. Table 3.10 presents the test program, and a total of 36 experimental cases were conducted for the main experiment.

In summary, a series of efforts and preparations were made for the main experiment. To address the boundary effect in the rigid box, a 5cm sponge was attached to the walls of shaking direction. The physical model accurately replicated the features of the prototype. Specifically, numerical analysis, approximate formulas, and sweep tests were conducted to replicate the natural frequency of the superstructure. The dynamic soil pressure was measured using a dynamic earth pressure measuring system comprising a combination of load cells, accelerometers, and loadcell plates. Additionally, a preliminary test was conducted to eliminate the inertial forces of the load cell plate and accurately measure the pure dynamic soil pressure from the ground. The soil was prepared in a dense state with a relative density of 80.63%. Figure 3.22 represents the typical layout of the main experiment conducted using a 1-g shaking table, illustrating an example of a High-rise building with basements (HB).

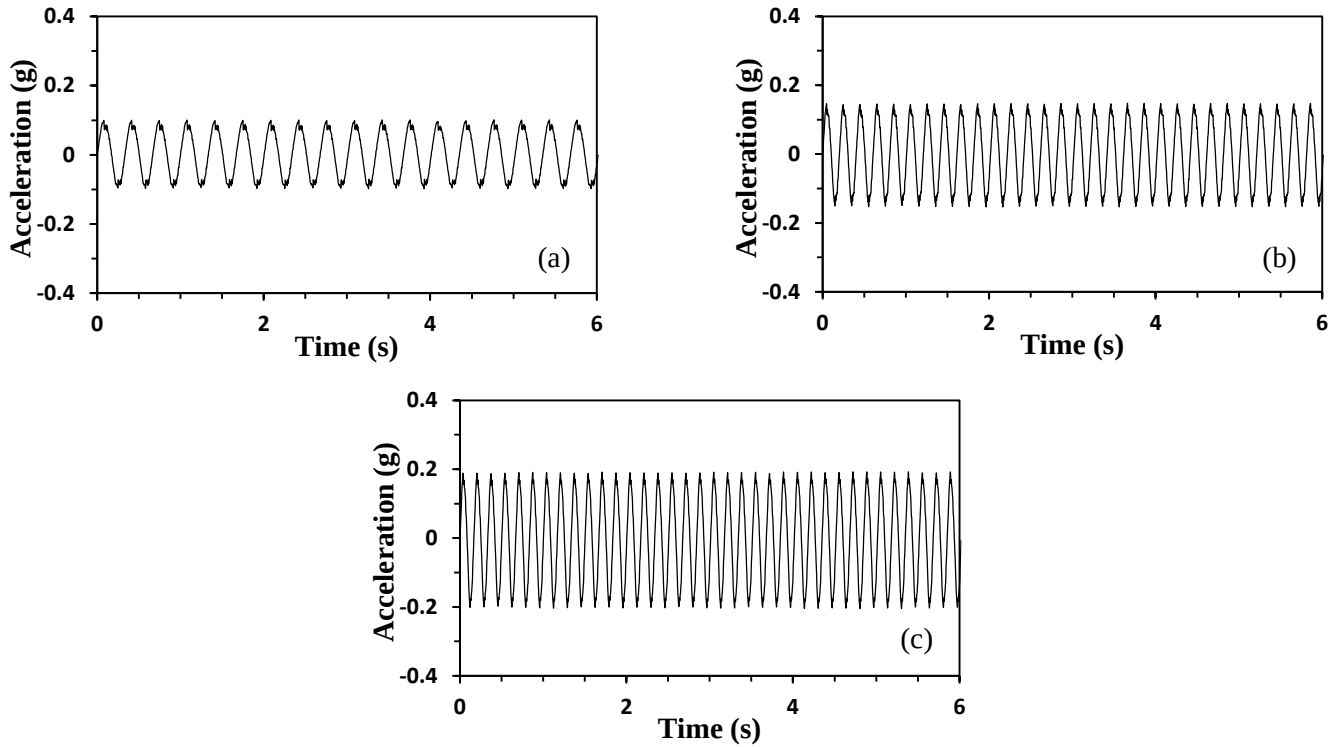

Figure 3.21 Input motions: (a) sine wave 3Hz 0.10g, (b) sine wave 5Hz 0.15g, and (c) sine wave 6Hz 0.20g

Table 3.10 Test program

Input motion		Physical model
Frequency (Hz)	Amplitude (g)	
3	0.1	No superstructure
5	0.15 0.2	3-Story superstructure
6	0.3	9-Story superstructure

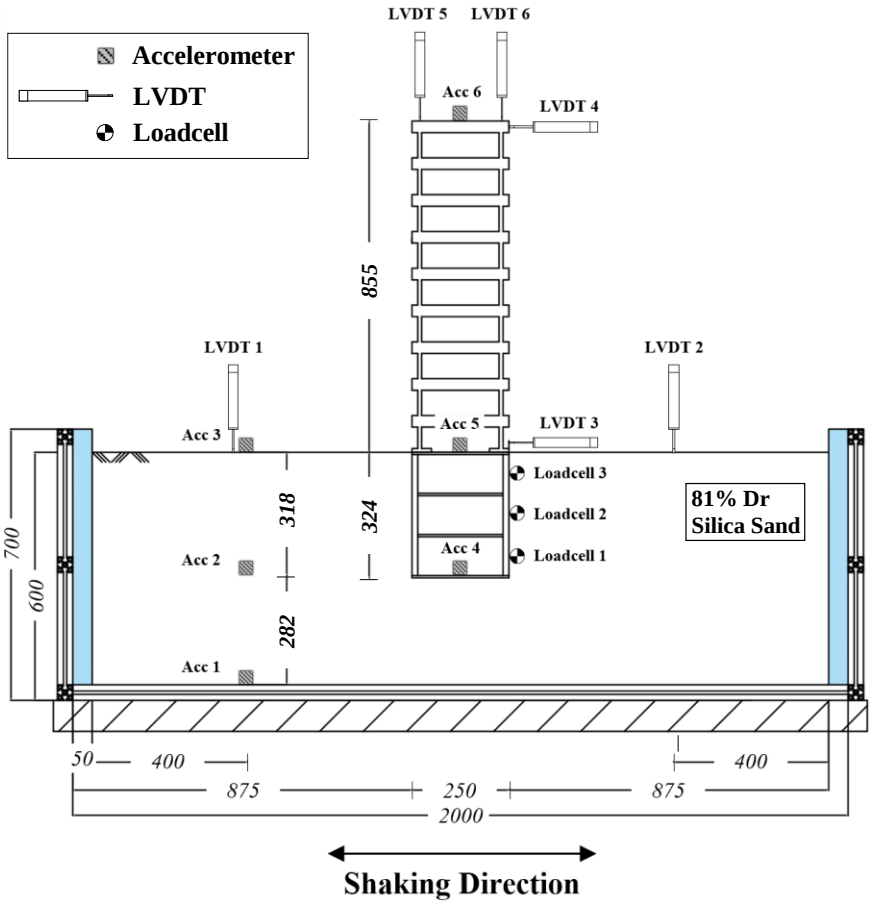

Figure 3.22 Layout of 1-g shaking table test showing the positions of measuring instrument and physical model. All dimensions are in mm.

Chapter 4 Evaluation of Seismic Earth Pressures on Basement Walls of Buildings

4.1 Introduction

Recently, numerous studies have been conducted on Soil-Structure Interaction (SSI) to accurately predict the response of structures, considering the complex interaction between structures and the soil. However, research on dynamic earth pressure acting on basement walls of buildings remains insufficient. It is anticipated that the dynamic earth pressure on basement walls significantly influences the behavior of the superstructure. However, current design codes rely on the Mononobe-Okabe (M-O) method, which does not consider this. Therefore, this study investigated the dynamic earth pressure acting on basement walls by varying the number of stories in the superstructure and subjecting it to seismic waves with different characteristics.

First, the study was conducted on the seismic behavior of buildings. Next, the influence of the number of stories in the superstructure on the dynamic pressure distribution was discussed. Additionally, the effect of the number of the superstructure stories on the magnitude of seismic pressure was investigated. Lastly, the seismic earth pressure coefficient based on the peak ground acceleration at the surface and the number of stories in the superstructure was proposed for the seismic design of basement walls.

4.2 Seismic Behavior of Buildings

A comparison of structural responses was conducted to understand the overall dynamic responses of buildings, specifically focusing on the free-field peak ground acceleration and the maximum acceleration at the top of the structure. This analysis allowed for the examination of the lateral behavior and dynamic pressure of the structure based on the number of superstructure stories.

Figure 4.1 compares the lateral displacement at the top of the structure with respect to the free-field peak ground acceleration (PGA_{ff}). No significant differences were observed based on the frequency of the seismic waves. Under the conditions of BO and LB, smaller displacements were observed, while HB exhibited significantly larger horizontal responses. Therefore, it was confirmed that the lateral displacement increases as the number of stories in the structure increases.

Figure 4.2 shows the dynamic thrust based on the maximum acceleration at the top of the structure. As the height of the structure increased, the horizontal displacement at the top was amplified, resulting in enhanced inertial forces in the superstructure and an increased magnitude of dynamic thrust.

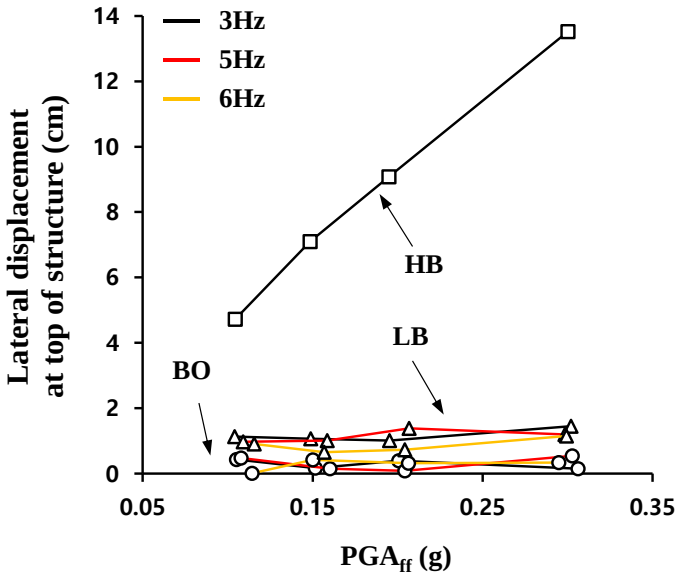

Figure 4.1 Comparison of lateral displacements according to the superstructure height

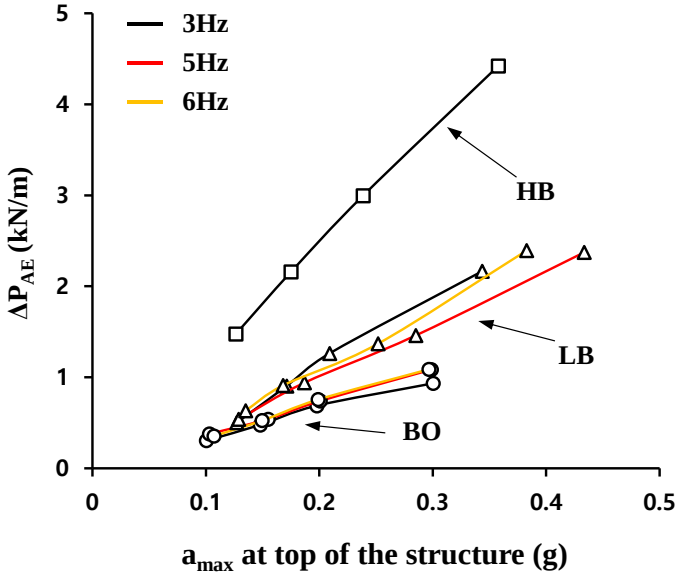

Figure 4.2 Comparison of dynamic thrusts according to the superstructure height

4.3 Seismic Earth Pressure Distribution

Figure 4.3 shows the distribution of dynamic thrust at a sine wave frequency of 3Hz. Similar to previous model test results, the Basement only case exhibited a triangular distribution where the dynamic thrust increases with depth (Al-Atik & Sitar, 2010; Candia & Sitar, 2013; Mikola & Sitar, 2013). This shape corresponds to the distribution predicted by the Mononobe-Okabe (M-O) method, which was the initial study conducted on dynamic thrust.

However, the results of the Low-rise building with basements (LB) and High-rise building with basements (HB) cases, which include the superstructure, exhibited different distributions compared to the previous case. As the number of floors in the superstructure increases, the distribution of dynamic thrust changed from a triangular shape to an inverted triangular shape. This pattern aligned with the distribution proposed by Seed & Whitman (1970), even though it did not specifically consider the presence of the superstructure. The increase in the number of stories in the superstructure corresponds to an increase in both the mass and height of the structure. Mass directly influences the inertial forces, while greater height leads to amplification of acceleration, resulting in higher accelerations. Consequently, the increased inertial forces exerted significant dynamic thrust on the basement wall near the ground surface, leading to a reverse triangular distribution of dynamic earth pressures.

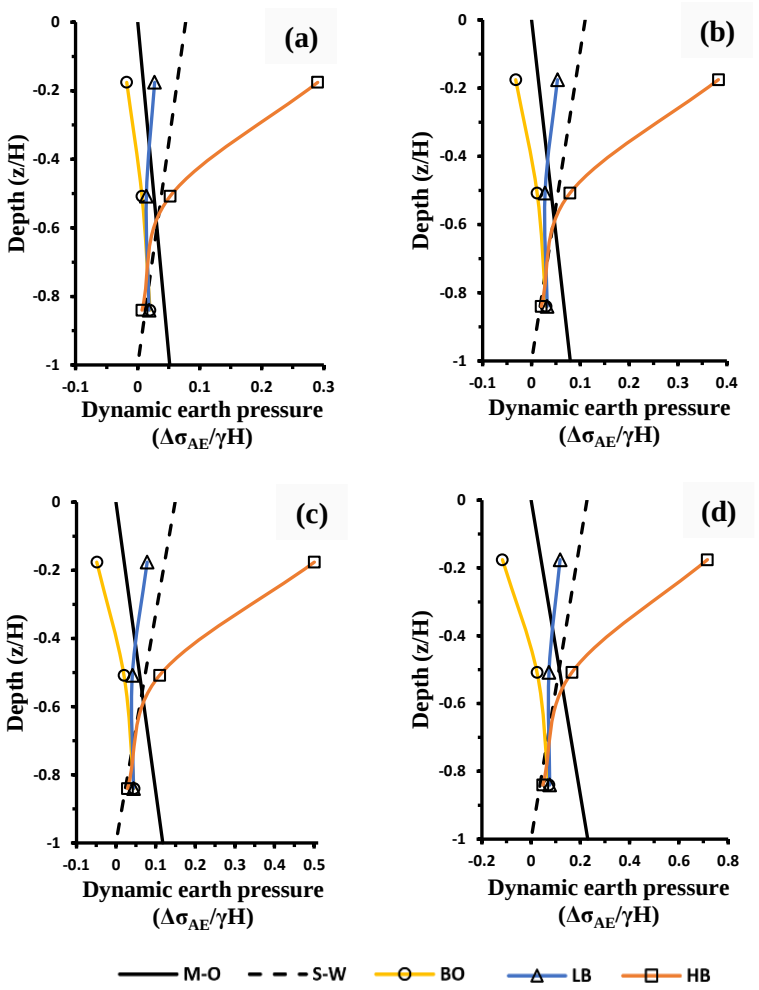

Figure 4.3 Dynamic earth pressure distribution according to the number of stories in the superstructure at the maximum total earth pressure for Sine Wave 3Hz: (a) 0.10g, (b) 0.15g, (c) 0.20g, and (d) 0.30g.

Figure 4.4 represents the distribution of dynamic earth pressure under a 5Hz sine wave. In the case of the Basement only, the distribution showed a triangular shape with maximum dynamic earth pressure occurring at the bottom of the basement, consistent with previous findings. However, as the number of stories in the superstructure increased, the distribution transitioned into a reverse triangular shape. The natural frequency of the High-rise Building (HB) was found to be 6.39Hz. Since the 5Hz sine wave is close to the natural frequency of HB, it induced slight resonance. Consequently, it was observed that the dynamic earth pressure acting on the basement wall located near the ground surface increased due to the inertial forces of the upper structure.

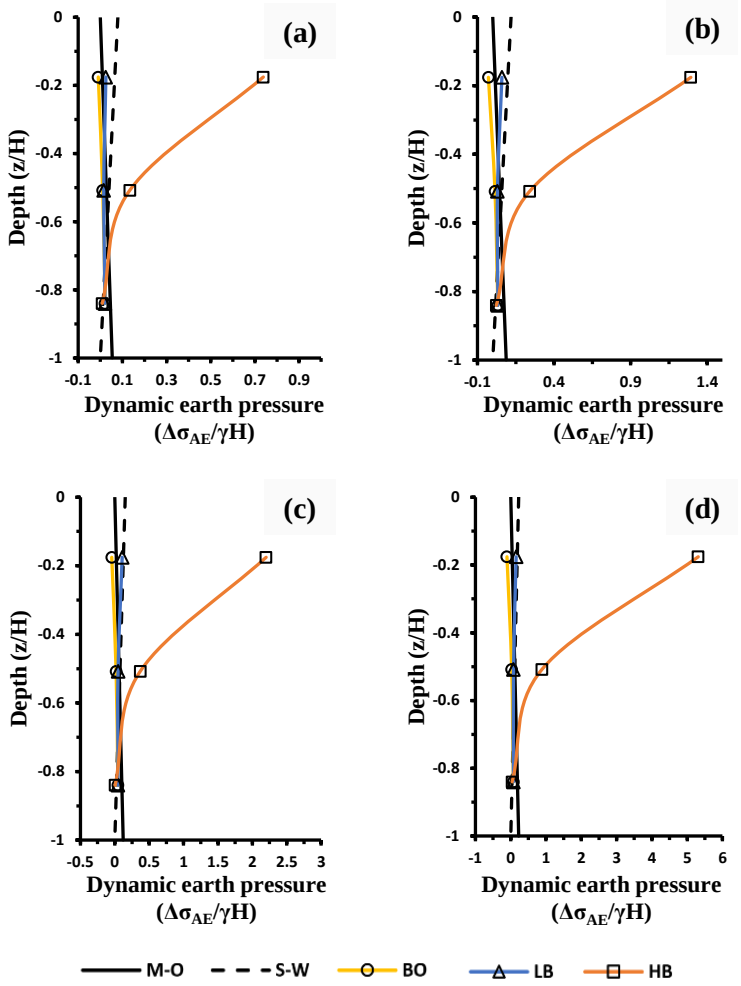

Figure 4.4 Dynamic earth pressure distribution according to the number of stories in the superstructure at the maximum total earth pressure for Sine Wave 5Hz: (a) 0.10g, (b) 0.15g, (c) 0.20g, and (d) 0.30g.

The distribution of dynamic earth pressure under a 6Hz sine wave is shown in Figure 4.5. The seismic load generated by a sine wave with a frequency component very close to the natural frequency of the HB structure clearly induced resonance. As a result, significant dynamic earth pressure acted not only on the basement wall adjacent to the ground surface but also on the walls of the middle-depth basement layer. Furthermore, this phenomenon was more pronounced with increasing amplitude of the input motion. Therefore, it was observed that when the natural frequency of the structure closely matched the frequency component of the seismic wave, the dynamic earth pressure acting on the basement wall increased significantly due to the resonance phenomenon in the superstructure.

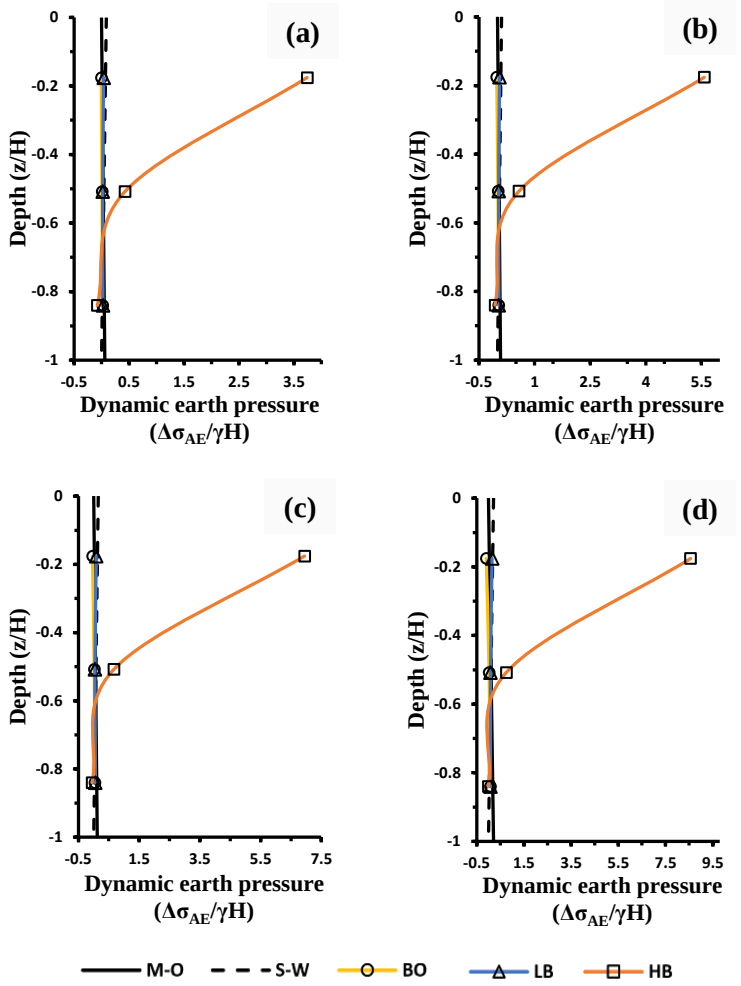

Figure 4.5 Dynamic earth pressure distribution according to the number of stories in the superstructure at the maximum total earth pressure for Sine Wave 6Hz: (a) 0.10g, (b) 0.15g, (c) 0.20g, and (d) 0.30g.

4.4 Seismic Earth Pressure Magnitude

Figure 4.6 presents the seismic earth pressure coefficient as a function of the free field PGA for the seismic earth pressure magnitude. In addition to the experimental results of this study, the figure also includes the Seismic earth pressure coefficients proposed by analytical methods such as the M-O method (1929), Seed & Whitman (1970), Wood (1973), as well as MOLIT (2019). Mikola & Sitar (2013) proposed equations for the seismic earth pressure coefficient based on PGA for non-displacing basements, providing both mean and upper bound values, which are also compared in the figure.

Figure 4.6 (a) represents the results for the basement only case. It showed a monotonic increase in the seismic earth pressure coefficient with increasing PGA. Additionally, our results yielded smaller coefficients compared to the mean proposed by Mikola & Sitar (2013). However, the upper bound from their study were applicable to our experimental results. Therefore, Seed & Whitman (1970) was also appropriate as the upper limit for this experimental result.

Figure 4.6 (b) shows the results for the Low-rise building with basements (LB). As the PGA magnitude increased, it exhibited a similar monotonic increasing trend as observed in the BO results. However, the values were generally higher compared to the BO case. This indicated that the inertial forces of the superstructure have a significant influence on the magnitude of dynamic earth pressure.

The results for High-rise building with basements (HB) are shown in Figure 4.6 (c). In the case of 5Hz and 6Hz sine waves, which closely match the natural frequency of the 9-story structure, they exhibit a different trend from the overall pattern. Therefore, only the results for 3Hz and 10Hz are shown. HB exhibited higher values compared to BO and LB. This indicates that the increased number of superstructure stories induced greater inertia, resulting in a more significant manifestation of dynamic earth pressure.

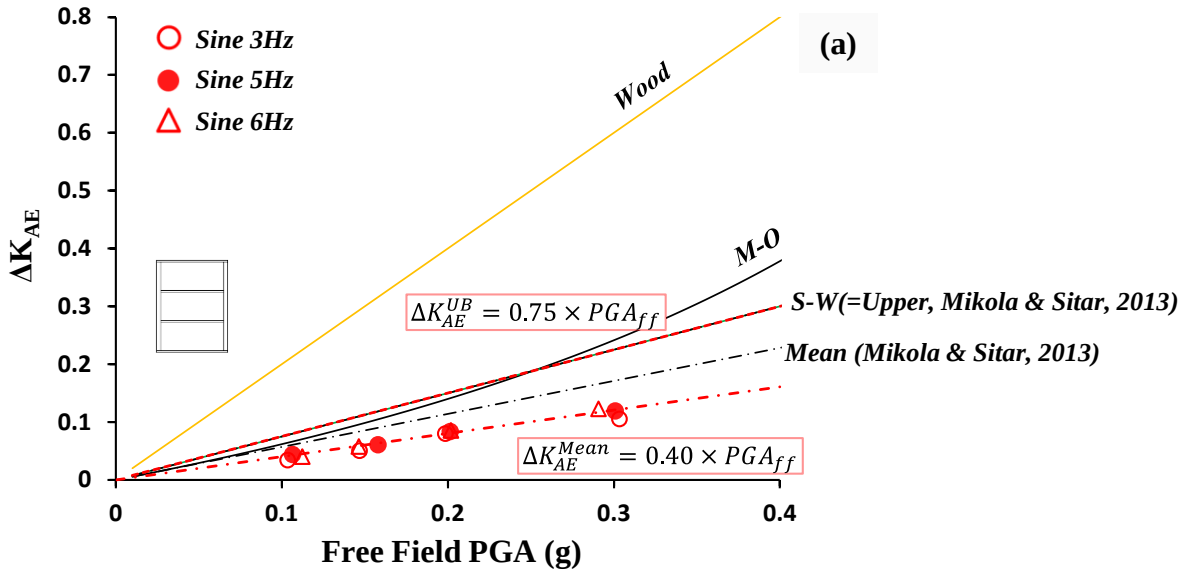
(a)
Sine 3Hz
Sine 5Hz
Sine 6Hz
Wood
M-O
S-W(=Upper, Mikola & Sitar, 2013)
Mean (Mikola & Sitar, 2013)
$\Delta K_{AE}^{UB} = 0.75 \times PGA_{ff}$
$\Delta K_{AE}^{Mean} = 0.40 \times PGA_{ff}$
ΔK_{AE}
0.8
0.7
0.6
0.5
0.4
0.3
0.2
0.1
0
0
0.1
0.2
0.3
0.4
Free Field PGA (g)

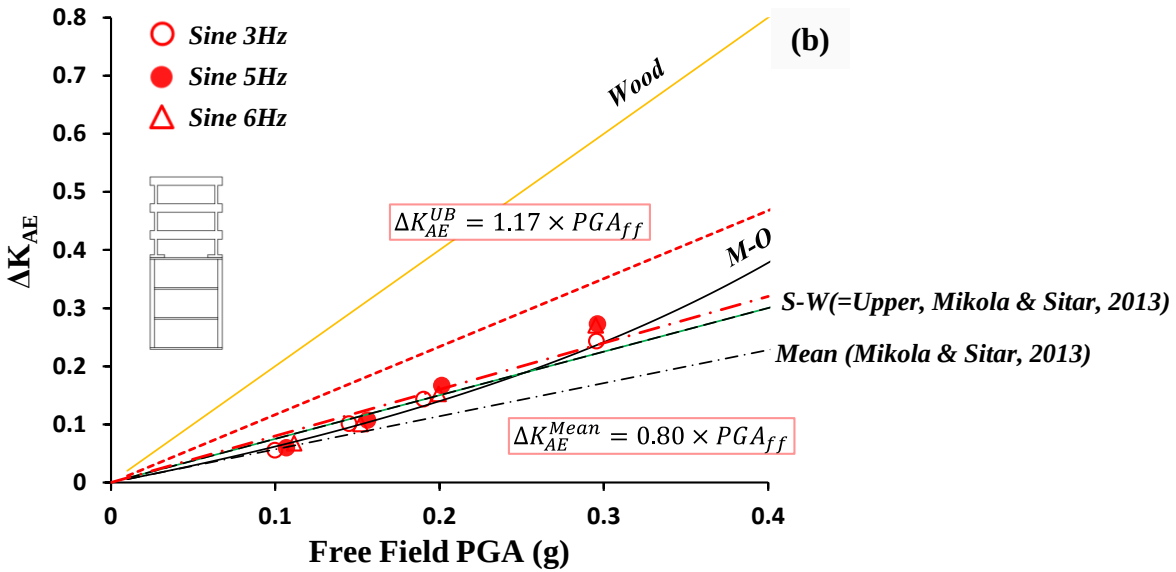
(b)
Sine 3Hz
Sine 5Hz
Sine 6Hz
Wood
M-O
S-W(=Upper, Mikola & Sitar, 2013)
Mean (Mikola & Sitar, 2013)
$\Delta K_{AE}^{UB} = 1.17 \times PGA_{ff}$
$\Delta K_{AE}^{Mean} = 0.80 \times PGA_{ff}$
ΔK_AE
Free Field PGA (g)
0
0.1
0.2
0.3
0.4
0.5
0.6
0.7
0.8

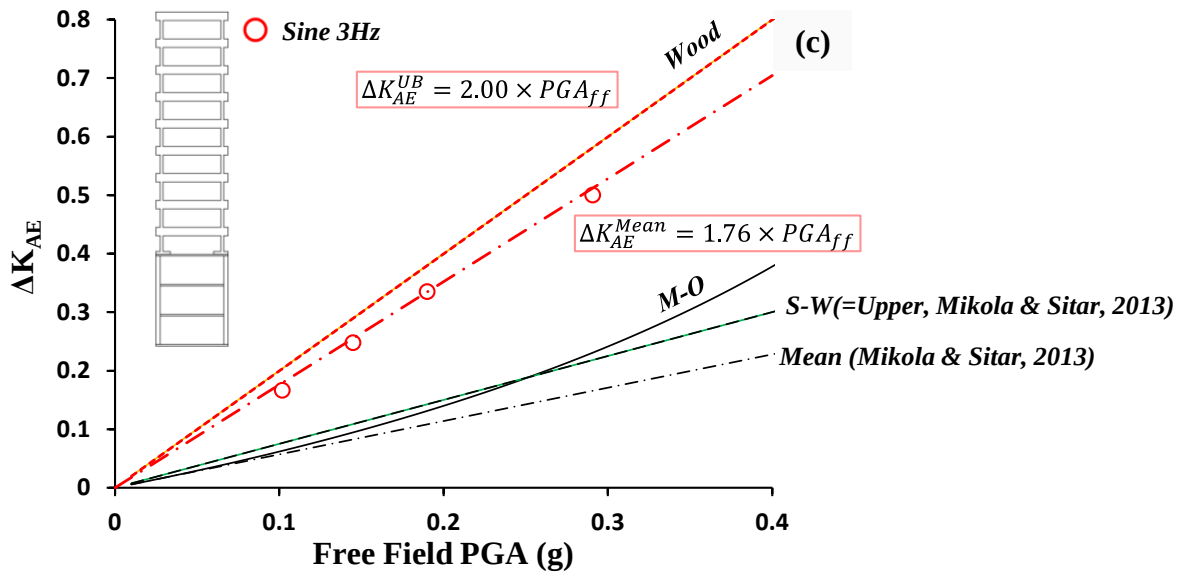

Figure 4.6 Seismic earth pressure coefficient as a function of PGA_{ff} for (a) Basement Only (BO), (b) Low-rise building with basements (LB), and (c) High-rise building with basements (HB)

Based on the results, the mean for each result was determined as a function of PGA_{ff}. Additionally, a proposed seismic earth pressure coefficient was introduced for the seismic design of basement walls, taking into account the maximum ground acceleration at the surface and the number of stories in the superstructure. For basement only (BO) case, a proportional constant of 0.75 suggested by Seed & Whitman (1970) was adopted, while for the High-rise building with basements (HB) case, a proportional constant of 2.00 proposed by Wood (1973) was used. As for the M-O method, exponential increase was observed from a PGA of 0.4g according to several references, whereas our study results showed a monotonic increasing trend. Therefore, an upper bound was proposed with the number of superstructure stories as a variable in a linear function. The proposed formula is as follows:

$$\Delta K_{AE}^{UB} = (0.14N + 0.75) \times PGA_{ff} \tag{4.1}$$

Where, N = the number of superstructure stories

PGA_{ff} = maximum ground acceleration at the free field

The seismic earth pressure coefficient, varying with the number of superstructure stories, was presented in Figure 4.6 based on the proposed formula. The upper bound for LB, determined by the proposed formula, was considered appropriate.

This study presented the results of the maximum dynamic earth pressure acting on basement walls of buildings using a series of seismic waves.

Depending on the phase relationship between the inertial forces and the dynamic earth pressure, the dynamic earth pressure can act as an additional load or a bearing capacity. Therefore, as a further study, it is necessary to perform a time history analysis of the inertial forces of the structure and the dynamic earth pressure acting on the basement wall to investigate their phase relationship. Additionally, since this experiment used only sine waves, further verification should be conducted using real seismic waves that include a variety of amplitudes and frequencies.

Chapter 5 Conclusions

The existing design codes provided the dynamic soil pressure acting on basement walls of buildings using the equivalent static analysis method, but it did not consider Soil-Structure Interaction (SSI). In this study, the number of superstructure stories and the characteristics of seismic waves were considered as influencing factors of seismic earth pressure. Seismic earth pressure acting on basement walls of buildings was investigated through 1-g shaking table tests. physical models were developed based on the similarity law applied, and especially the natural frequencies of the superstructure were appropriately determined through numerical analysis, approximate formulas, and sweep tests. The dynamic earth pressure, which is of utmost importance in the experiments, was measured using a dynamic earth pressure measuring system consisting of accelerometers, load cells, and a load cell plate. Preliminary experiments allowed obtaining modified forces by removing the inertia forces from the loadcell plate. This enabled the acquisition of several results, including the acceleration response at the top of the structure and the free-field acceleration. The main conclusion drawn from the experiments are summarized below.

(1) The analysis of seismic behavior of buildings based on the number of superstructure stories was performed. It was observed that the lateral displacement at the top of the structure increased with the number of stories, while no significant differences were found based on the seismic vibration frequency. The dynamic thrust, determined by the maximum acceleration at the

top of the structure, also increased with the height of the structure. This suggests that the inertia of the superstructure plays a crucial role in the magnitude of dynamic thrust acting on basement walls.

(2) The seismic earth pressure distribution in the basement only condition exhibited the typical triangular shape observed in previous studies. However, as the number of superstructure stories increased, the distribution transformed into an inverted triangular shape. Thus, it has been confirmed that the increased mass and amplified acceleration resulting from the increased number of superstructure stories contribute to an increase in inertia, leading to a substantial dynamic soil pressure on the basement walls near the ground surface.

(3) The magnitude of dynamic soil pressure was expressed using the seismic earth pressure coefficient, and in all cases, it exhibited a monotonic increase as the PGA increased. In the case of basement only, the results aligned with previous studies confirming that Seed & Whitman (1970) provided an appropriate upper bound. However, in the presence of a superstructure, the coefficient surpassed the values obtained from previous studies, and its magnitude increased with the number of stories. Therefore, it was confirmed that the inertia of the superstructure influences the magnitude of dynamic soil pressure, and its impact increases with the number of stories.

(4) A seismic earth pressure coefficient was proposed for the seismic design of basement walls of buildings, considering the number of stories in the superstructure and the maximum ground acceleration at the surface. The proposed formula suggested an upper bound by using a function with the number of superstructure stories as the variable.

References

Al Atik, L., & Sitar, N. (2010). Seismic earth pressures on cantilever retaining structures. Journal of geotechnical and geoenvironmental engineering, 136(10), 1324-1333.

ASCE. (2016). Minimun design loads for buildings and other structures. ASCE/SEI 7-16. Virginia: American Society of Civil Engineers.

Candia, G., & Sitar, N. (2013). Seismic earth pressures on retaining structures in cohesive soils. UC Berkeley.

Coulomb, C.A. (1776). Essai sur une application des regles de maximis et minimis quelques problemes de statique, relatits a l'architecture. Memoires de Mathematique de l'Academie Royale pres Divers Savants Vol.7.

FEMA. (2009). NEHRP Recommended Seismic Provisions for New Buildings and Other Structures. FEMA P-750. Washington DC: Federal Emergency Management Agency.

Hokmabadi, A. S., Fatahi, B., & Samali, B. (2014). Assessment of soil–pile–structure interaction influencing seismic response of mid-rise buildings sitting on floating pile foundations. Computers and Geotechnics, 55, 172-186.

Iai, S. (1989). Similitude for shaking table tests on soil-structure-fluid model in 1g gravitational field. Soils and Foundations, 29(1), 105-118.

Kramer, S. L. (1996). Geotechnical earthquake engineering. Pearson Education India.

Matsuo, H. (1941). Experimental study on the distribution of earth pressure acting on a vertical wall during earthquakes. J. of the Japan Society of Civil Engrg, 27(2).

Mikola, R. G., & Sitar, N. (2013). Seismic earth pressures on retaining structures in cohesionless soils. California Department of Transportation.

MOLIT(Ministry of Land, Infrastructure and Transport). (2019). Korean seismic building design code. KDS 41 17 00 (in Korean)

Mononobe, N., & Matsuo, H. (1929). On the determination of earth pressure during earthquakes. Proceedings of the World Engineering Conference, 9.

NIST. (2012). Soil-structure interaction for building structures. Report No. NIST GCR 12-917-21. Maryland: NEHRP Consultants Joint Venture.

Okabe, S. (1926). General theory on earth pressures and seismic stability of retaining wall and dam. Journal of the Japan Society of Civil Engineering, 10(6), 1277-1323.

PEER. (2017). Guidelines for performance based seismic design of tall buildings. Report No. 2017/06. Berkeley CA: Pacific Earthquake Engineering Research Center.

Seed, H. B., & Whitman, R. V. (1970). Design of earth retaining structures for dynamic loads. Proc. ASCE Specialty Conf. on Lateral Stresses in the Ground and Design of Earth Retaining Structures. Vol.1, Cornell Univ., Ithaca, N.Y., 103–147.

Segaline, H., Saez, E., & Ubilla, J. (2022). Evaluation of dynamic soil-structure interaction effects in buildings with underground stories using 1 g physical experimentation in a transparent shear laminar box. Engineering Structures, 266, 114645.

SH. (2019). Building Structure Guidelines. Report No. SH-SD-G001-0.

Turan, A., Hinchberger, S. D., & El Naggar, M. H. (2013). Seismic soil–structure interaction in buildings on stiff clay with embedded basement stories. Canadian Geotechnical Journal, 50(8), 858-873.

Wood, J.H. (1973). Earthquake induced soil pressures on structures," Ph.D Thesis. California Institute of Technology, Pasadena, CA.

Yang, E. K., Choi, J. I., Han, J. T., & Kim, M. M. (2010). Evaluation of dynamic group pile effect in sand by 1 g shaking table tests. Journal of the Korean Geotechnical Society, 26(8), 77-88.

초 록

황태훈
건설환경공학부
서울대학교 대학원

지진 발생시 건축물 지하층 외벽에 작용하는 동적토압은 구조물의 안정성에 심각한 피해를 입힐 수 있다. 또한, 지반과 구조물 사이에 작용하는 상호작용은 동적토압에 큰 영향을 미치는 것으로 알려져 있다. 건축물의 지하층과 같은 지하구조물에 작용하는 동적토압의 결정을 위해 많은 연구가 수행되었다. 이중 등가정적해석 기반 동적토압 산정법이 주로 사용되었으며, 한국을 포함한 여러 국가의 내진 설계기준에서 동적토압의 결정방법으로 채택하고 있다. 하지만, 도심지에 건설된 지하층을 포함한 구조물은 대부분 다층으로 구성된 상부구조를 포함하고 있다. 이러한 건축물은 지진시 상부구조의 진동으로 인한 관성력 등 지반-구조물 상호작용으로 인해 지하층에 작용하는 동적토압에 복합적인 영향을 미친다. 그러나, 등가정적해석 기반 동적토압 산정법은 지반-구조물 상호작용으로 인한 영향을 전혀 고려하지 않고 있으며, 설계기준에서조차 지반-구조물 상호작용의 중요성을 언급할 뿐 구체적인 적용방법을 제시하지 못하고 있는 실정이다. 따라서, 지하층구조에 작용하는 동적토압에 대해 지반-구조물 상호작용의 영향을 반영하는 연구가 필요하다.

본 연구에서는 상부 구조물의 높이와 입력파의 특성이 동적토압에 미치는 영향을 분석하기 위하여 1-g 진동대 모형실험을 수행하였다. 모형 구조물은 원형의 고유주기, 높이 그리고 질량에 대한 상사법칙을 만족하도

록 제작하였고, 상부 구조물 높이에 따라 상부 구조물 없이 지하층만 존재하는 형태, 지상 3층 및 9층에 해당하는 세 가지 모형을 사용하였다. 모형 지반은 진동대 시험장비의 진동을 이용하여 상대밀도 약 80%인 조밀한 사질토 단일층으로 조성하였다. 입력파는 진동수 및 최대가속도에 따라 16개의 정현파로 구성하여 토조바닥에서부터 가력하였다. 동적토압은 지하층 구조물 외벽에 설치된 로드셀을 통해 계측하였고, 가속도계와 변위계를 사용하여 모형 지반 및 구조물의 지진 거동을 측정하였다.

실험 결과, 구조물의 수평거동은 상부 구조물의 층수에 따라 증가하였다. 또한, 지하층만 존재하는 경우 동적토압분포는 지반 내 깊어질수록 커지는 삼각형 형태를 띠는 것에 비해 상부 구조물이 높아질수록 점차 지표면 부근이 커지는 역삼각형 형태로 변화하는 것을 확인하였다. 이와 함께, 상부 구조물 높이에 따라 제시한 동적수평토압증분계수를 통해 상부 구조물의 높이가 높아질수록 발생하는 동적토압이 증가하는 것으로 나타났으며, 상부 구조물 영향을 고려하지 않은 기존 연구에서 제안된 방법을 통해 예측한 토압에 비해 큰 값으로 나타났다. 마지막으로, 지표면 최대가속도 기반 상부 구조물 층수에 따른 동적수평토압증분계수를 제안하였다.

주요어: 지하층, 상부 구조물, 동적토압, 1-g 진동대 모형실험, 지반-구조물 상호작용

학번: 2021-20334

감사의 글

대학원에 입학하여 석사졸업까지 2년이란 시간이 지났습니다. 저에게 대학원 입학은 한 분야의 전문가로 성장하기 위한 첫걸음을 내딛는 순간이자 서울 생활의 시작을 의미했습니다. 캐리어 하나에 옷가지와 함께 꿈을 담아 상경했던 2021년 7월은 무척이나 더웠고, 새로운 시작은 설렘과 동시에 두려움으로 다가왔습니다. 하지만, 석사과정 동안 생각치도 못한 많은 발전을 경험하였고, 석사졸업을 앞둔 지금은 이루 말할 수 없을 만큼 기쁩니다. 감사의 글을 통해 기쁨과 함께 이 한편의 부족한 논문이 완성되기까지 지도해주시고 도움주신 분들에게 감사한 마음을 전달 드리고자 합니다.

먼저, 부족한 저를 성장시켜 주시고, 지도해주신 김성렬 교수님께 항상 진심으로 감사드립니다. 그리고 언제나 인자한 웃음으로 좋은 말씀해주신 정충기 교수님께 감사의 인사를 드립니다. 또한, 항상 자상하게 지도해주신 박준범 교수님께도 감사드립니다.

내진팀의 맏형으로 좋은 조언을 아낌없이 해주었던 유병수, Tran 형님과 곁에서 많은 도움을 주신 Buu 형님, 오승원 후배님에게 감사드립니다. 또한, 입학부터 졸업까지 가장 가까운 곳에서 동고동락했던 사수 황병윤 형님께 진심으로 감사한 마음을 전달 드립니다.

연구실 안과 밖에서 조언을 아끼지 않고 좋은 모범이 되어주신 구교영, 신규범, 홍성호, 정택규 형님과 항상 동생으로 다정하게 대해주신 조

범희, Rahim, 송영우, 홍승완, 김경선 형님께 감사드립니다. 또한, 언제나 웃는 얼굴로 맞이해준 한재인, 조기안, 이민호, 김준우와 류정현 형님께 고맙고, 입학부터 함께 달려온 동기 고석준, Aneesu는 졸업 후 새롭게 다가올 앞날에 좋은 일만 가득하길 바랍니다. 그리고 곁에서 항상 힘이 되어주고 행복한 연구실 생활을 영위하게 해준 존경하는 김인현 형님과 사랑스러운 윤형석 후배님께 진심으로 감사하며 앞으로 더욱 더 승승장구하길 바랍니다.

마지막으로, 무한한 사랑과 배려로 저에게 큰 힘이 되어주시는 아버지, 어머니와 언제나 멋있고 자랑스러운 황정의 형님께 이 논문을 바칩니다. 앞으로 제가 받은 행복보다 더 큰 행복으로 보답드리는 아들, 동생이 될 것을 약속드리며, 감사의 글을 마치겠습니다.